AD NUMBER

AD888561

LIMITATION CHANGES

TO:

Approved for public release; distribution is unlimited.

FROM:

Distribution authorized to U.S. Gov't. agencies only; Test and Evaluation; OCT 1971. Other requests shall be referred to Arnold Engineering Development Center, Attn: XON, Arnold AFS, TN 37389.

AUTHORITY

AEDC ltr, 14 Jul 1972

PERFORATED WALL NOISE IN THE AEDC-PWT 16-FT AND 4-FT TRANSONIC TUNNELS

O. P. Credle

ARO, Inc.

October 1971

PROPULSION WIND TUNNEL FACILITY
ARNOLD ENGINEERING DEVELOPMENT CENTER
AIR FORCE SYSTEMS COMMAND
ARNOLD AIR FORCE STATION, TENNESSEE

NOTICES

When U. S. Government drawings specifications, or other data are used for any purpose other than a definitely related Government procurement operation, the Government thereby incurs no responsibility nor any obligation whatsoever, and the fact that the Government may have formulated, furnished, or in any way supplied the said drawings, specifications, or other data, is not to be regarded by implication or otherwise, or in any manner licensing the holder or any other person or corporation, or conveying any rights or permission to manufacture, use, or sell any patented invention that may in any way be related thereto.

Qualified users may obtain copies of this report from the Defense Documentation Center.

References to named commercial products in this report are not to be considered in any sense as an endorsement of the product by the United States Air Force or the Government.

FOREWORD

The work presented herein was sponsored by Headquarters, Arnold Engineering Development Center (AEDC), Air Force Systems Command (AFSC), under Program Element 65401F, System 921E.

The results reported herein were obtained by ARO, Inc. (a subsidiary of Sverdrup & Parcel and Associates, Inc.), contract operator of AEDC, AFSC, Arnold Air Force Station, Tennessee, under Contract F40600-72-C-0003. This work was conducted under ARO Projects PT2059, PB1963, and PT2129 from September 1969 to December 1970, and the manuscript was presented for publication on August 23, 1971.

This technical report has been reviewed and is approved.

George F. Garey
Lt Colonel, USAF
AF Representative, PWT
Directorate of Test

Joseph R. Henry
Colonel, USAF
Director of Test

ABSTRACT

This report presents the results of recent studies of noise in Propulsion Wind Tunnel (16T) and Aerodynamic Wind Tunnel (4T). Noise levels in the free stream and at the test section wall were measured in both tunnels as a function of Mach number, Reynolds number, wall angle, and wall porosity. In Tunnel 4T, free-stream noise characteristics were also evaluated with solid (taped) test section walls. Test results revealed that the perforated test section wall holes generate discrete frequency, high energy noise. In Tunnel 16T, there is a critical Mach number range in which a wall hole frequency is in acoustic resonance with a compressor blade frequency. Test section noise levels were found to vary slightly with wall angle and significantly with Mach number and wall porosity. The wall porosity corresponding to the minimum noise levels was found in Tunnel 4T. For Mach numbers greater than 0.90, the minimum noise condition was found to correspond to the optimum aerodynamic porosity. For subsonic Mach numbers the minimum noise condition corresponded to a porosity setting that was slightly less than the optimum aerodynamic porosity. It is shown that the noise levels in transonic tunnels with perforated walls can be reduced, and specific recommendations are made to "detune" Tunnel 16T in the critical Mach number range.

CONTENTS

APPENDIXES

I. ILLUSTRATIONS

Figure

NOMENCLATURE

a_∞	Free-stream speed of sound, ft/sec
b	Diameter, ft

ΔC_p	Dynamic pressure coefficient, $(\tilde{p}/q) \times 100$, percent
$\Delta \overline{C}_p$	Spatial average of ΔC_p, percent
d	Perforated wall hole diameter, ft
f	Frequency, Hz
Δf	Analyzer bandwidth, Hz
G(f)	Power spectral density (psd) function, $\left[\tilde{p}(f)^2\right]/\Delta f$, psf^2/Hz
H	Shape factor, δ^*/θ
$\overline{H}$	Spatial average of shape factor of all four walls
h	Separation distance between leading and trailing edge of a slanted hole, d/cos 60 deg, ft
M_∞	Test section free-stream Mach number
M_{wall}	Local wall Mach number, $\overline{U}_{wall}/\alpha_\infty$
N	Tunnel 16T compressor speed, rpm
n	Edge tone stage, 1, 2, 3, or 4
$\hat{p}$	Time average or mean pressure, $\frac{1}{T}\int_0^T p(t)dt$, psf
$\tilde{p}$	Root-mean-square (rms) fluctuating pressure, $\left[\frac{1}{T}\int_0^T p^2(t)dt\right]^{1/2}$, psf
p_c	Tunnel plenum pressure, reference pressure, psfa
p_t	Free-stream total pressure, psfa
p(t)	Instantaneous, time-dependent fluctuating pressure, psf
q	Free-stream dynamic pressure, psf
Re/ft	Unit Reynolds number, U_∞/ν_∞, 1/ft
S	Strouhal number, $f \cdot b/U_\infty$
S_d	Edge tone number, $f \cdot h/\overline{U}_{wall}$
t	Time, sec
U_{wall}	Average velocity at the measuring point closest to the test section wall, ft/sec
$\overline{U}_{wall}$	Spatial average of wall velocity on all four test section walls, ft/sec

U_∞	Average free-stream velocity, ft/sec
u(y)	Average longitudinal boundary-layer velocity as a function of distance from the test section wall, ft/sec
v_o	Average velocity normal to the test section wall, positive velocity indicates inflow, ft/sec
x	Longitudinal distance, ft
y	Transverse distance from test section wall, ft
δ	Boundary-layer thickness, in.
δ^*	Boundary-layer displacement thickness, in.
$\bar{\delta}^*$	Spatial average of the displacement thickness on all four test section walls, in.
θ	Boundary-layer momentum thickness on the test section wall, in.
$\bar{\theta}$	Spatial average of the momentum thickness on all four test section walls, in.
θ_w	Tunnel 16T east and west wall angle setting, Tunnel 4T top and bottom wall angle setting, positive angle indicates wall deflection away from tunnel centerline, deg
ν_∞	Free-stream kinematic viscosity, ft^2/sec
τ	Wall porosity, percent

SECTION I
INTRODUCTION

The use of ventilated test section walls in transonic wind tunnels has been found to be an effective technique for maintaining the desired steady-state aerodynamic conditions in the test region. However, these walls have also been found to be capable of generating high energy noise levels, and in many cases, these noise levels are of sufficient magnitude to degrade the accuracy and thus the quality of the test data. As a part of recent efforts to improve the state of the art in transonic testing, Ref. 1, the problem of wall noise has been investigated during the course of a number of acoustic studies in Tunnels 16T and 4T.

This report presents the results of these studies with emphasis on the wall noise levels generated in the test section and the possible techniques for reducing these levels. The results are limited by the inability to completely isolate the individual influence parameters in the wind tunnels. However, a better understanding of the noise generating mechanism of perforated walls has been obtained. In addition, it is shown that wall noise can be reduced below the present levels, and that for some conditions it is possible to reduce these noise levels to those of a smooth wall tunnel.

SECTION II
EXPERIMENTAL INVESTIGATION

2.1 DESCRIPTION OF TUNNEL 16T

The AEDC Propulsion Wind Tunnel (16T) is a variable density, continuous flow tunnel capable of operation at Mach numbers from 0.20 to 1.60 at stagnation pressures up to 4000 psfa. The test section is 16 ft square by 40 ft long and is enclosed by perforated walls of fixed 6-percent porosity. The sidewalls of the test section are movable to allow various wall angle settings as an aid in minimizing wall interference at supersonic Mach numbers. Details of the test section are shown in Fig. 1 (Appendix I), and a section of the perforated walls and the geometry details of the holes and the hole pattern are shown in Fig. 2.

The tunnel airflow is established with a single compressor shown schematically in Fig. 3. The compressor is driven at a constant speed

of 600 rpm for $M_\infty \geq 0.60$. Test section Mach number is set by controlling the test section pressure ratio via the remotely controllable compressor stator blades for subsonic Mach numbers, and by the proper combination of stator blade angle, nozzle contour, and plenum static pressure for transonic Mach numbers. The plenum static pressure is controlled by the plenum evacuation system, PES. A more complete description of the tunnel performance capabilities may be found in Ref. 2.

2.2 DESCRIPTION OF TUNNEL 4T

The AEDC Aerodynamic Wind Tunnel (4T) is a variable density, continuous flow tunnel and is capable of operation over a Mach number range from 0.10 to 1.30 at stagnation pressures from 300 to 3700 psfa. The test section is 4 ft square by 12.5 ft long as shown in Fig. 4, and is equipped with variable porosity perforated walls with an available porosity range from 0- to 10-percent open area. The top and bottom walls are hinged in Tunnel 4T in a manner similar to the sidewalls of Tunnel 16T. The geometry details of the perforated walls are shown in Fig. 5.

The tunnel airflow is established by a suitable number of PES compressors. These compressors operate at constant speed and blade angle or pressure ratio. The test section nozzle contour is fixed, and Mach number is set by throttling with a downstream butterfly valve and by maintaining the proper plenum pressure. Plenum pressure is controlled by the combination of a single PES compressor pumping on the plenum cavity and by diffuser flaps downstream of the test section.

The test section wall porosity settings versus Mach number have been determined based on minimizing the wall interference effects on a nonlifting model, Ref. 3. The recommended optimum porosity schedule is listed in Table I (Appendix II) for selected Mach numbers.

Flow conditioning features in Tunnel 4T include turbulence damping screens and an acoustic silencer upstream of the stilling chamber. A more complete description of the tunnel is included in Ref. 2.

2.3 GENERAL TEST PROCEDURE

The tests described in the sequel were conducted to evaluate the flow quality in the test sections of Tunnels 16T and 4T. Three different

calibration models have been used to measure the free-stream noise levels: (1) a 10-deg cone with flats, Fig. 6, (2) a 10-deg transition cone, full body of revolution, Fig. 7, and (3) a 2-in. ogive cylinder, Fig. 8. Model number 2 was also used to measure the free transition length in each tunnel, and model number 3 has been flight tested and will be used to develop a test section noise criteria. Note (Fig. 8) that the nose of the 2-in. ogive cylinder was gritted to ensure that all noise data were obtained under the same near-field boundary-layer noise conditions.

The results of a number of the studies using models 1 and 2 to measure test section flow quality are included in Refs. 4 through 7. The general test procedure in each of these studies was to obtain a quantitative evaluation of the noise and transition characteristics while varying a single test section variable or parameter such as Mach number, total pressure, wall angle, or wall porosity. In many cases, these are not truly independent variables, however, and this complicates the interpretation of the data and renders it very difficult to evaluate the perforated walls as a source of the distrubances in the tunnels. It was found that the noise levels measured with each model were different for identical tunnel conditions. The 10-deg transition cone measured the highest overall levels (which is attributed to noise generated by the traversing probe support structure) and the 2-in. ogive cylinder measured the lowest overall levels for the same frequency passband. This additional complication renders it necessary to make quantitative comparisons of amplitudes with identical acoustic measurement bodies. The measured frequencies were found to be invariant with model geometry.

2.4 TUNNEL 16T STUDIES

Each of the three models have been used to evaluate the flow quality in Tunnel 16T. The models were instrumented as shown in Figs. 6, 7, and 8. Instrumentation in addition to that in the models included wall boundary-layer rakes on all four walls, test section wall dynamic pressure transducers at stations -10 and 12, and transducers in the plenum chamber, the stilling chamber, and upstream and downstream of the main compressor. The wall boundary-layer data and the effect of small changes in compressor blade angle were obtained during the study with the 10-deg transition cone. The noise characteristics of the tunnel compressor were obtained during the study with the 10-deg cone with flats. Test section wall, plenum chamber, and stilling chamber data were obtained during all three studies.

Instrumentation for the acquisition and analysis of the fluctuating dynamic data included the transducer and microphone systems, on-line rms detectors for the computation and tabulation of the overall rms levels, and an FM magnetic tape recorder. All magnetic tape data were analyzed off line using a constant bandwidth analog power-spectral-density (psd) analyzer. A typical instrumentation system is shown in Fig. 9.

2.5 TUNNEL 4T STUDIES

The same three models were also used to evaluate the flow quality in Tunnel 4T. The tests were similar in the two tunnels with the exception that the wall boundary-layer data were obtained during the study using the 2-in. ogive cylinder.

The comparison of data from the various studies that have been conducted in Tunnel 4T is complicated by changes in the test section walls and in the plenum cavity. However, the measured differences in noise characteristics as a result of these various changes provide valuable insight into techniques for reducing noise. The original study, Ref. 4, was conducted with one-third of the perforated wall holes plugged, and the cut-off plate motion was downstream. For this original configuration, the holes were fully open at approximately 6.6-percent porosity. The second study, Ref. 6, was conducted with all holes open, and the cut-off plate motion was upstream. For this final configuration, the holes were fully open at 10-percent porosity. These two configurations are compared in Fig. 10 where the difference in the geometry of the open area in the hole is shown for intermediate porosities. For the most recent study using the 2-in. ogive cylinder, the interior walls of the plenum enclosure had been treated with a sound absorbing acoustic material for the reduction of internal as well as external noise levels. Thus from the basis of a representative description of existing Tunnel 4T noise, primary emphasis will be placed on the results of the most recent study.

The tunnel variables that were evaluated in Tunnel 4T included Mach number, total pressure, wall angle, and wall porosity. Wall porosity was varied from 10 to 0 percent and, in addition, an evaluation was conducted over the Mach number range from 0.30 to 0.80 with all four walls taped smooth on the airstream side. A photograph of the taped test section walls is shown in Fig. 11.

Instrumentation for the acquisition and analysis of fluctuating dynamic data in Tunnel 4T was similar to the Tunnel 16T instrumentation.

2.6 PRECISION OF MEASUREMENTS

The estimates of errors in the steady-state data as determined from instrumentation and calibration inaccuracies are as follows:

Parameter	Accuracy
M_∞	±0.002
p_t	±4 psf
θ_w	±0.03 deg
τ	±0.02 percent

The accuracy of the tabulated on-line rms data as measured by the pressure transducers is estimated to be ±0.4 db or ±2.0 psf at a sound pressure level of 160 db. These estimates are based on a confidence level of 95 percent.

The uncertainty of the frequency analysis based on a 67-percent confidence level was established as follows:

From 30 to 500 Hz	11.1 percent
From 500 Hz to 10 kHz	3.53 percent

SECTION III
ANALYSIS

3.1 BOUNDARY-LAYER CHARACTERISTICS

A comprehensive analysis of the test section wall boundary-layer characteristics is beyond the scope of this report. It is helpful, however, to consider the wall boundary layer in terms of certain basic parameters that are derived from the momentum and energy equations. These parameters can be calculated as approximations from pressure measurements in actual boundary layers.

From Ref. 8 the boundary-layer displacement thickness δ^* is defined as

$$\delta^* = \int_0^\delta \left[1 - \frac{u(y)}{U_\infty}\right] dy \qquad (1)$$

where y equals the distance from the boundary and δ is the distance at which $\frac{u(y)}{U_\infty} = 0.999$. The displacement thickness represents the distance that the streamlines are shifted because of the formation of the boundary layer. The momentum thickness, which is an indication of the loss of momentum in the boundary layer relative to potential flow, is defined as

$$\theta = \int_0^\delta \frac{u(y)}{U_\infty}\left[1 - \frac{u(y)}{U_\infty}\right] dy \tag{2}$$

The boundary-layer shape factor is defined as

$$H = \frac{\delta^*}{\theta} \tag{3}$$

These definitions apply to both laminar and turbulent boundary layers.

For a laminar boundary layer on a flat plate at zero incidence, and uniform suction, the two-dimensional equations of motion can be solved for the velocity profile as

$$u(y) = U_\infty\left[1 - \epsilon^{v_o (y)/\nu_\infty}\right] \tag{4}$$

The boundary conditions at y = 0 are u = 0, v = v_o = constant < 0, and it is assumed that the velocity gradient in the x direction is zero, or $\partial u/\partial x = 0$. In this solution v_o is the velocity normal to the wall, and for suction or flow out of the boundary, $v_o < 0$. This velocity profile can be used to compute the displacement and momentum thicknesses in the laminar boundary layer as

$$\delta^* = \frac{\nu_\infty}{-v_o} \tag{5}$$

$$\theta = \frac{1}{2}\left(\frac{\nu_\infty}{-v_o}\right) \tag{6}$$

Equations (5) and (6) indicate that δ^* and θ are both inversely proportional to the suction velocity v_o. From Eq. (4) as v_o decreases (increased suction), u(y) increases. Note also that if δ^* or θ are measured in a laminar boundary layer, and ν_∞ is known, then v_o can be computed.

The theoretical description of a turbulent boundary layer requires the solution of the integral momentum and energy equations, rather than partial differential equations as was the case for the laminar boundary layer. However, the analytic expressions for the stream and dissipation functions that are required for the solution in turbulent flow cannot

be determined theoretically. Thus the calculation procedure for turbulent boundary layers is a semiempirical one based on experimental data. For the present study it is sufficient to note that because of the similarity of the forcing function and velocity profiles in the laminar and turbulent case that the same relative variations can still be expected to occur; i.e., in the case of the turbulent boundary layer as with the laminar boundary layer an increase in the suction velocity $-v_o$ is evidenced by an increase in u(y) and a decrease in δ^*. The semiempirical solutions in a turbulent boundary layer indicate that separation occurs for a shape factor of

$$H = 1.8 \text{ to } 2.4 \tag{7}$$

The description of the pressure fluctuations generated by a turbulent boundary layer is equally difficult and can only be determined by empirical techniques at this time. In Ref. 9, an empirical formula for the prediction of the pressure fluctuations beneath a turbulent boundary layer is given as

$$\Delta C_p = 0.6/(1 + 0.14\ M_\infty^2) \tag{8}$$

where

$$\Delta C_p = \left(\frac{\tilde{p}}{q}\right) \times 100 \text{ percent}$$

This relation is based on the assumption of a constant static pressure through the boundary and an adiabatic wall. The values of ΔC_p that are computed from Eq. (8) can be considered as a lower limit for wind tunnel noise levels.

3.2 RIGID BODY FLOW INTERACTION

The phenomenon of rigid body flow interaction and the generation of sound or pressure disturbances has been the subject of numerous theoretical and experimental investigations. As is usually the case, however, the investigations were limited to a single variable and simplified configurations that are not representative of wind tunnel geometries. The results are of value in a relative evaluation of tunnel noise and in the isolation of sources.

The generation of the well-known Karman vortex sound or aeolian tone is determined by flow around a cylinder or other body of revolution, Ref. 10. The Karman vortex exhibits a constant frequency scaling parameter or Strouhal number given by

$$S = \frac{fb}{U_\infty} \tag{9}$$

where b is the rod diameter in feet, f is the vortex frequency in Hz, and U_∞ is the approach velocity in ft/sec. The Karman vortex tone is generated by the transverse oscillatory motion of the wake behind a body. This is a result of vortices shedding off the body alternately on one side and then the other. The periodicity and frequency of these vortices results in a tone that is audible to the human ear. The width of the discrete frequency is controlled by the aerodynamic damping which increases with increasing Reynolds number.

When the Karman vortex is subjected to an external sound source with a frequency close to that of the vortices, then the magnitude of the tone is amplified and a stimulated vortex tone or a high intensity resonant whistle is generated. This resonant whistle also generates strong higher order harmonics. The external source can be an acoustic disturbance in the airstream or a downstream body interacting on the upstream one, e. g., an array of rods or cylinders.

An edge tone can also be generated in a moving medium. In this case directed flow or a jet impinges upon a sharp edge or wedge, Refs. 11 through 14. The exact mechanism by which the disturbance is generated is not as well understood as that of the Karman vortex tone. However, recent work, Refs. 12, 13, and 14, suggests that the mechanism is a combination of a Karman vortex at the edge feeding back as an acoustical pressure source to the jet. The edge tone occurs at frequencies for which the "edge-less" jet is most sensitive to acoustic disturbances. By considering the feedback loop, a phase criterion can be determined such that the permissible frequencies are shown to occur at fixed stages. Experimental data have shown that at each stage, the frequency varies continuously as the velocity is varied. The stages are not harmonically related, but are separated by hysteretic jumps, and it is possible for a number of stages to be excited at once. If an external acoustic disturbance is present, or a resonant column is introduced, it is possible for the level of a given stage to be amplified, and harmonics of that stage generated in a manner similar to the resonant whistle of the Karman vortex.

The experimental investigations of the edge tone have been used in Ref. 7 to formulate an empirical relation for the prediction and correlation of the numerous discrete frequencies measured in wind tunnels. This relation is given as

$$\frac{fh}{U_\infty} = 0.15 \frac{n^{1.68}}{(M_\infty + 1)} \qquad (10)$$

with $n = 1, 2, 3, 4$

where:

f	frequency of fluctuations, Hz
h	resonant hole separation, i.e., the distance between the leading and trailing edge of the perforated wall hole, ft
M_∞	free-stream Mach number
U_∞	free-stream velocity, ft/sec

For 60-deg slanted hole walls,

$$h = d/\cos 60\text{-deg} = 2d \tag{11}$$

SECTION IV
RESULTS AND DISCUSSION

4.1 TUNNEL 16T NOISE AND WALL BOUNDARY-LAYER CHARACTERISTICS

Typical results of the Tunnel 16T studies are shown in Figs. 12 through 17. The variations in overall noise levels and wall boundary-layer characteristics as a function of Mach number are shown in Fig. 12. Note that as discussed in Ref. 5, the noise levels are a maximum in the Mach number range from 0.70 to 0.75 with an increase of approximately a factor of three over the minimum levels. The displacement thickness, the longitudinal mean velocity at the wall as measured by the rake pitot probe that was closest to the wall, and the shape factor are all presented in terms of the average of the measured or computed values on all four walls. Although the boundary-layer characteristics of the four walls were about equal, Ref. 6, it was found that a spatial average was more representative than a single wall value in analyzing test section centerline effects, and that an improved comparison between tunnels was possible. As noted in Fig. 12, the variations of δ^* with M_∞ are much less than the variations in ΔC_p with M_∞. The wall velocity and the shape factor both increase uniformly with M_∞ with no apparent correlation with ΔC_p.

Frequency spectra of the signals obtained on the 10-deg cone with flats at selected Mach numbers and at two different values of total pressure are shown in Fig. 13. Note that a strong broadband frequency component at a center frequency of about 600 Hz is controlling the maximum overall noise levels in the critical Mach number range as noted in Fig. 12. It was found that the center frequency of this component changed with Mach number but was invariant with total pressure,

and thus Reynolds number. The width, and in some cases the amplitude, of this broadband component was reduced with increasing total pressure. Finally, the presence of strong higher order harmonics of this frequency is noted in the critical Mach number range. As Mach number is increased to 0.90 and above, the low frequency fundamental disappears, and a predominate high frequency component at 2.0 to 3.0 kHz is detected. This high frequency component also moves directly with Mach number, but is at a much lower amplitude than the lower frequency component. Thus the increase in noise level as controlled by the strong 550- to 650-Hz frequency component is fundamental to the test section noise in Tunnel 16T. A number of studies have been directed toward determining the source of this component. If the amplitude of this component could be reduced or eliminated, a considerable reduction in the tunnel noise levels would be realized.

One such study was the measurement of the noise levels around the entire tunnel circuit. The results of these measurements are shown in Fig. 14. The frequency spectra are compared at six different locations throughout the tunnel for Mach number variations from 0.60 to 1.30. The comparison is relative to frequencies only and not amplitude. Note that in the critical Mach number range the predominate frequency is close to the second harmonic of the compressor blade fundamental frequencies (310 and 330 Hz) and that there are strong harmonics of the approximately 600-Hz fundamental in the test section. The movement of the predominate frequency with Mach number and the presence of strong harmonics suggests that a resonant condition exists.

In an attempt to verify this conclusion, two separate studies were conducted using the main compressor. The first was to vary the compressor stator blade angle a small amount and to compensate for the resultant change in pressure ratio by increasing or decreasing plenum suction. The second study was to trip the compressor off line while on test conditions and to record the noise levels at the outset of the compressor coast. The plenum pressure was again used to hold test section conditions for the first 30 sec of the coast. The results of these two evaluations of the noise characteristics in the test section are shown in Fig. 15 for a restricted range, narrow band analysis of the frequency spectra. Note that these narrow band analyses reveal a broadband frequency component with a narrow band frequency or pure tone superimposed. The results of the blade angle investigation, Fig. 15a, indicate that the pure tone frequency moves with blade angle, but the center frequency of the broadband component is invariant. The former observation demonstrates that the compressor is the source of this pure tone. The latter observation verifies that the test section Mach number was constant. As the frequency of the pure tone moves to coincidence with

the center frequency of the broadband component, the broadband level is constant ($M_\infty = 0.75$). The results obtained by reducing compressor speed, Fig. 15b, indicate that the frequency of the pure tone is reduced with decreasing compressor speed, but the broadband frequency is stationary. These studies support the conclusion that a resonant condition exists in the critical Mach number range, but do not explain the mechanism responsible for this condition or the fact that the resonance is excited by a pure tone that is slightly less than the calculated compressor second harmonic. It is apparent, however, that the compressor is the forcing function and that high noise levels are present when the test section characteristic frequencies are close to a compressor controlled frequency.

The evaluation of the effect of wall angle on the noise and wall boundary characteristics for $M_\infty = 1.05$ and 1.20 is shown in Figs. 16 and 17. Note that for both Mach numbers the level of ΔC_p is relatively unchanged with θ_w, although there is a significant change in the value of δ^*. Thus, ΔC_p is insensitive to variations in δ^* when the variations are controlled by changes in θ_w. It is shown in Fig. 16 that increasing the wall angle produces a decreasing value of $\overline{U}_{wall}$ and, as shown in Fig. 17, a corresponding decrease in the broadband at the predominate frequency of 2.5 kHz.

4.2 TUNNEL 4T NOISE AND WALL BOUNDARY-LAYER CHARACTERISTICS

Representative results of the Tunnel 4T studies are shown in Figs. 18 through 25. The Tunnel 4T studies were much more comprehensive than those in Tunnel 16T in that the effect of changing wall porosity was evaluated as well as the evaluation of the noise and wall boundary-layer characteristics with the test section walls taped. For the taped wall evaluation, a fabric backed vinyl tape was used on the interior side of the walls, and the walls were closed to 0-percent porosity to minimize the pressure differential across the tape.

Noise levels and boundary-layer characteristics as a function of Mach number are shown in Fig. 18 for wall porosities of 10 percent, 6 percent, and the optimum porosity values for aerodynamic testing as listed in Table I, Appendix II. Also shown for comparison purposes are results obtained with the walls taped. Note that for $M_\infty < 1.0$ there is a reduction in ΔC_p and δ^* when τ is reduced from 10 to 6 percent. Note also that $\overline{U}_{wall}$ and $\overline{H}$ are both invariant with wall porosity at the subsonic Mach numbers. The results in Fig. 18a for $\tau = 10$ percent indicate that separation in the wall boundary layer occurs as evidenced

by the abrupt change in $\overline{H}$ and the corresponding break in the $\overline{U}_{wall}$ curve, although this is not reflected in a change in ΔC_p. The overall trends of ΔC_p with Mach number for τ = 6 percent and optimum are essentially the same as those for 16T, but the noise levels are found to be significantly higher for τ = 10 percent. Finally, there is a definite indication that with the proper choice of porosity the test section noise levels can be reduced considerably at all Mach numbers, and in some cases approach those of a smooth wall tunnel.

The analyses of the frequency spectra of the noise signals at selected Mach numbers and wall porosities of 6 percent and optimum are shown in Fig. 19. The higher levels of ΔC_p at subsonic Mach numbers for optimum τ are shown to originate from a strong low frequency component in the 800- to 900-Hz range. Note that with the exception M_∞ = 0.80, higher harmonics are noticeably absent. As Mach number is increased, this low frequency component disappears and a higher frequency component appears in a manner similar to Tunnel 16T. The low frequency component is a function of porosity, but the high frequency component is not. Finally, the high frequency component reveals a higher order mode that is not harmonically related to the fundamental frequency.

A comparison of the frequency spectra for τ = 6.0 percent and the walls taped is shown in Fig. 20. Observations of significance include a definite reduction in the high frequency broadband noise, the elimination of the controlling discrete frequencies, and the identification of certain discrete frequencies that are not generated by the perforated walls. In particular, it is shown that there is a discrete frequency in the spectra with the taped walls that varies from 1.6 kHz at M_∞ = 0.30 to 3.5 kHz at M_∞ = 0.80. This variation with Mach number is much more extreme than the variations of the low or high frequency components previously discussed for the open wall condition. In addition, the frequency is much too high for a duct mode, and has not been detected from earlier measurements upstream in the stilling chamber, or upstream of the silencer, Ref. 15. Finally, there is a fixed 3.5-kHz frequency component that is invariant with Mach number. These same frequencies were present in the spectra obtained on the test section wall. The source of these frequencies is unknown at this time although, based on the results of Ref. 15, it appears that they do not originate upstream of the test section.

The variations of test section noise, wall boundary-layer characteristics, and frequency spectra with wall angle are shown in Figs. 21 and 22 for optimum wall porosity. In general, the trends are found to

be similar to those in Tunnel 16T. An evaluation at a subsonic Mach number, $M_\infty = 0.80$, is also included which was not available from the Tunnel 16T studies. The evaluation at a subsonic Mach number (Fig. 22a) reveals that the low frequency component is very sensitive to changes in wall angle, and strong harmonics are possible. The high frequency component and the higher order mode are also affected by changes in wall angle, but there is no evidence of harmonic content.

The evaluation of the effect of wall porosity variations is shown in Figs. 23 and 24. Included in Fig. 23 are the values of ΔC_p, δ^*, $\overline{U}_{wall}$, and $\overline{H}$ for taped walls. For $M_\infty = 0.50$ it is shown in Fig. 23a that the noise levels can be reduced to that of a solid wall tunnel with the proper selection of wall porosity. The minimum value of ΔC_p at $M_\infty = 0.50$ occurs at $\tau = 6$ percent, but is only slightly less than the value of ΔC_p for $\tau = 5$ percent which is the optimum porosity from an aerodynamic viewpoint. For $M_\infty = 1.0$ and 1.2, Figs. 23b and c, the minimum value of ΔC_p corresponds closely to that obtained at the optimum value of porosity. As noted in the Mach number evaluation, there is a significant increase in ΔC_p and δ^* and a decrease in $\overline{U}_{wall}$ as τ approaches 10 percent. The shape factor is seen to be constant with wall porosity. Frequency spectra for $M_\infty = 1.0$ at various wall porosities are shown in Fig. 24. The high frequency broadband component tends to increase in frequency with increasing wall porosity, but a lower frequency broadband component appears at about 1.4 kHz and decreases in frequency with increasing wall porosity.

The test section noise levels for the perforated walls with a porosity of 6.0 percent and for the taped walls are compared to the theoretical noise levels beneath a turbulent boundary layer, Eq. (8), in Fig. 25. Note that although the theory is for the noise levels under the boundary layer and the measured values are on the test section centerline and thus are influenced by all four walls, the taped wall values are approximately equal to the theoretical values at the lower Mach numbers. The deviation at $M_\infty = 0.70$ and 0.80 for taped walls is attributed to the previously discussed but unexplained discrete frequency component that moves to 3.5 kHz at $M_\infty = 0.80$.

4.3 COMPARISON OF TUNNELS 16T AND 4T

A comparison of the overall noise levels, ΔC_p, versus Mach number as obtained from the ogive cylinder in Tunnels 16T and 4T is shown in Fig. 26. In general, the noise levels are higher in Tunnel 16T, with a maximum ΔC_p of 2.45 percent, than in Tunnel 4T, where a maximum ΔC_p of 1.67 percent is noted.

The relative changes in the frequency spectra measured in Tunnels 16T and 4T for M_∞ and θ_W variations, and in Tunnel 4T for τ variations have been compared in an attempt to correlate the predominate frequencies in each tunnel to a common source mechanism. Since the frequency variations do not follow a vortex tone trend of constant Strouhal number, an edge tone source is assumed. If the previously discussed edge tone equation, Eq. (10), is applied directly, however, it is obvious that the use of U_∞ and M_∞ does not account for the observed frequency shifts with changes in θ_W and τ since in both cases U_∞ and M_∞ were held constant. Thus, a new empirical relationship is needed for predicting wall noise that is controlled by the near-field flow velocity. Such a relationship should not invalidate the results of Ref. 7, but rather support them. As a first try, a correlation function was attempted based on the average longitudinal velocity measured at a height corresponding to the displacement thickness of the boundary layer on each test section wall. The correlation was very poor between the two tunnels, however, and small changes in discrete frequencies were not detected.

The average value of the longitudinal velocity measured by the boundary-layer probe that was closest to each wall was considered next. This is a physically reasonable choice since this value is the best measurement of the velocity that a given hole actually sees. Using this velocity, an empirical relationship was found that was similar to Eq. (10) but uses $\overline{U}_{wall}$ and $\overline{M}_{wall}$ as the controlling variables, and has different constants. The new relationship is given as

$$S_d = f\,h/\overline{U}_{wall} = 0.16\,n^{1.55}/(0.70 + \overline{M}_{wall}) \qquad (12)$$

where

n = the edge tone stage

f = the measured frequency, Hz

$\overline{U}_{wall}$ = the spatial average of the longitudinal wall velocity, ft/sec

$\overline{M}_{wall} = \overline{U}_{wall}/a_\infty$

$h = 2d$, ft

Following rearrangement and substitution, Eq. (12) is given as

$$n^{1.55} = \frac{2df}{a_\infty \overline{M}_{wall}}\,(0.70 + \overline{M}_{wall})/0.16 \qquad (13)$$

In this form, each edge tone stage as a function of $\overline{M}_{wall}$ is represented by a straight line. The values of $n^{1.55}$ for n = 1, 2, and 3 are compared with the value of Eq. (13) that is computed from the measured frequencies and average wall velocities in Fig. 27 for Mach number variations in Tunnels 16T and 4T. The comparison reveals that the offending frequencies are originating from an edge tone type of mechanism. The comparison also reveals the excitation of multiple stages at once, and the presence of the harmonic of the first stage in Tunnel 16T. Thus the broadband frequency shown in Fig. 15 that is responsible for the high noise levels in Tunnel 16T is generated by a wall hole edge tone. The same condition is also seen to exist in Tunnel 4T with the first stage edge tone identified. There is a definite line shown in Fig. 27 between n = 2 and n = 3 which corresponds to the 4.0- to 5.0-kHz frequency detected in Tunnel 4T that does not correlate with an edge tone mode or a harmonic of some fundamental. The source of this frequency is known to be the walls, but the mechanism has not been identified. The primary source of noise however is the low frequency disturbance in the critical Mach number range, and this has been identified as a first stage edge tone in each tunnel. A similar conclusion was reached in Ref. 7 based on the correlation of a large number of transonic tunnels.

The same empirical relation, Eq. (13), is also applied to the measured variations in the frequency spectra and wall velocity for changes in θ_w and τ as shown in Fig. 28. Note that for $\overline{M}_{wall} = f(\theta_w)$ the correlation is very good, and that for $\overline{M}_{wall} = f(\tau)$ there is no correlation. This result is attributed to the fact that θ_w variations alter δ^* and $\overline{U}_{wall}$ without significantly changing the pressure drop across the walls and thus the mass flow through the holes. Variations in τ, however, change the pressure drop across the wall and result in changes in δ^* without a corresponding change in $\overline{U}_{wall}$. Thus the measured variations in the frequency spectra with changes in τ must be attributed to changes in the flow characteristics through the wall holes rather than across them. This conclusion is not surprising since the hole geometry changes with τ as noted in Fig. 10.

4.4 TECHNIQUES FOR REDUCING NOISE

The ultimate goal of the numerous acoustic studies that have been conducted is to acquire sufficient knowledge to reduce the test section noise levels in Tunnels 16T and 4T. Thus consideration should be given to the techniques that have been proved effective in reducing test section noise and to those that promise to be effective based on the results of this wall noise study.

As mentioned earlier and shown in Fig. 10, modifications were performed on the Tunnel 4T perforated walls to improve the test section aerodynamic flow quality. It was found that there had been a corresponding reduction in noise levels attributable to the wall modifications as shown in Fig. 29 where a significant reduction in frequency amplitude and density is noted. Based on these data, and the results of varying wall porosity, it can be concluded that the optimum test section aerodynamic conditions will approach the conditions for minimum noise levels. It can also be concluded that a restriction in each hole as in Tunnel 4T is better than the open holes in Tunnel 16T. For round holes, a variable porosity, with an available range of τ that is greater than that required, and upstream motion of the cut-off plate results in reduced test section noise levels.

The reduction in the test section wall noise levels attributed to the plenum cavity acoustic insulation is shown in Fig. 30. Note that although the discrete frequencies are not changed, the broadband and the low frequency levels have been reduced. On the basis of classical room acoustics, and from the results of this comparison, it is concluded that test section noise reduction techniques should include a test section enclosure with high acoustic absorption characteristics.

The acoustic resonance in Tunnel 16T in the critical Mach number range and the absence of downstream propagating compressor related frequencies in the test section of Tunnel 4T demonstrates the need for a silencer in reducing test section noise levels.

A technique for reducing the noise levels consists of modifications to the existing walls and could be accomplished without a major redesign. Since the abrupt geometry of the hole edge and the sharp downstream lip are responsible for the generated noise levels, alterations to the hole edges are indicated. Two such alterations are (1) rounding each hole edge, thus giving each hole an indistinct profile, and (2) serrating the lip of each hole. The justification for the first alteration is found in Fig. 31 where an oil smear flow visualization of the wall flow in Tunnel 4T is shown. Note the flow concentration at the hole edges and the eddies propagating downstream from each hole. The second alteration is analogous to the installation of flow spoilers on a weir crest to eliminate the so-called nappe oscillations over a dam spillway, Ref. 16.

SECTION V
CONCLUSIONS

The noise characteristics generated by perforated test section walls in Tunnels 16T and 4T have been evaluated. Based on a number of studies, it was concluded that:

1. The maximum noise levels were controlled by edge tones generated by the sharp edges of the inclined holes in the test section walls.
2. In Tunnel 16T the first stage edge tone was in harmonic resonance with a compressor generated acoustic frequency.
3. In Tunnel 4T the first stage edge tone was controlling the overall noise levels, but was not in resonance with any known external source frequency.
4. The test section noise levels were reduced in Tunnel 4T when the wall geometry was modified, and the porosity adjusted for optimum aerodynamic conditions. For some conditions, the resultant noise levels were found to be equal to those of a smooth wall tunnel.
5. The random noise levels in the test section of Tunnel 4T were reduced by the installation of acoustic insulation on the interior walls of the plenum cavity.

REFERENCES

1. Transonic Aerodynamic Testing - A State-of-the-Art Assessment, "A Preliminary Report of the NASA-U.S. Air Force Ad Hoc Group on Transonic Scale Effects and Test Techniques." April 27, 1970.
2. Test Facilities Handbook (Ninth Edition). "Propulsion Wind Tunnel Facility, Vol. 4." Arnold Engineering Development Center, July 1971.
3. Jacocks, J. L. "Evaluation of Interference Effects on a Lifting Model in the AEDC-PWT 4-Ft Transonic Tunnel." AEDC-TR-70-72 (AD868290), April 1970.

4. Credle, O. P. "An Evaluation of the Fluctuating Airborne Environment in the AEDC-PWT 4T Transonic Tunnel." AEDC-TR-69-236 (AD861673), November 1969.

5. Credle, O. P. and Shadow, T. O. "Evaluation of the Overall Root-Mean-Square Fluctuating Pressure Levels in the AEDC PWT 16-Ft. Transonic Tunnel." AEDC-TR-70-7 (AD864827), February 1970.

6. Credle, O. P. and Carleton, W. E. "Determination of Transition Reynolds Number in the Transonic Mach Number Range." AEDC-TR-70-218 (AD875995), October 1970.

7. McCanless, G. F., Jr. "Additional Correction of 4% Saturn V Protuberance Test Data." Technical Report HSM-R1-71, NAS8-30517, January 21, 1971.

8. Schlichting, H. "Boundary Layer Theory." McGraw Hill, 6th Edition, 1968.

9. Lowson, M. V. "Prediction of Boundary Layer Pressure Fluctuations." AFFDL-TR-67-167, April 1966.

10. Morse, P. M. and Ingard, K. O. "Theoretical Acoustics." McGraw Hill, 1967.

11. Brown, G. B. "On Vortex Motion in Gaseous Jets and the Origin of their Sensitivity to Sound." The Proceedings of the Physical Society, Vol. 47, Pt. 4, July 1935, pp. 703-732.

12. Brown, G. B. "The Vortex Motion Causing Edge Tones", The Proceedings of the Physical Society. Vol. 49, Pt. 5, September 1937, pp. 493-507.

13. Powell, A. "On the Edge Tone." JASA, Vol. 33, No. 4, April 1961, pp. 395-409.

14. Powell, A. "Vortex Action in Edge Tones." JASA, Vol. 34, No. 2, February 1962, pp. 163-166.

15. Credle, O. P. "Evaluation of the Acoustic Silencer in the AEDC-PWT 4-Ft. Transonic Tunnel." AEDC-TR-68-234 (AD841857), October 1968.

16. Schwartz, H. I. "Edgetones used Nappe Oscillations." JASA, Vol. 39, No. 3, 1966, pp. 579-582.

APPENDIXES
I. ILLUSTRATIONS
II. TABLES

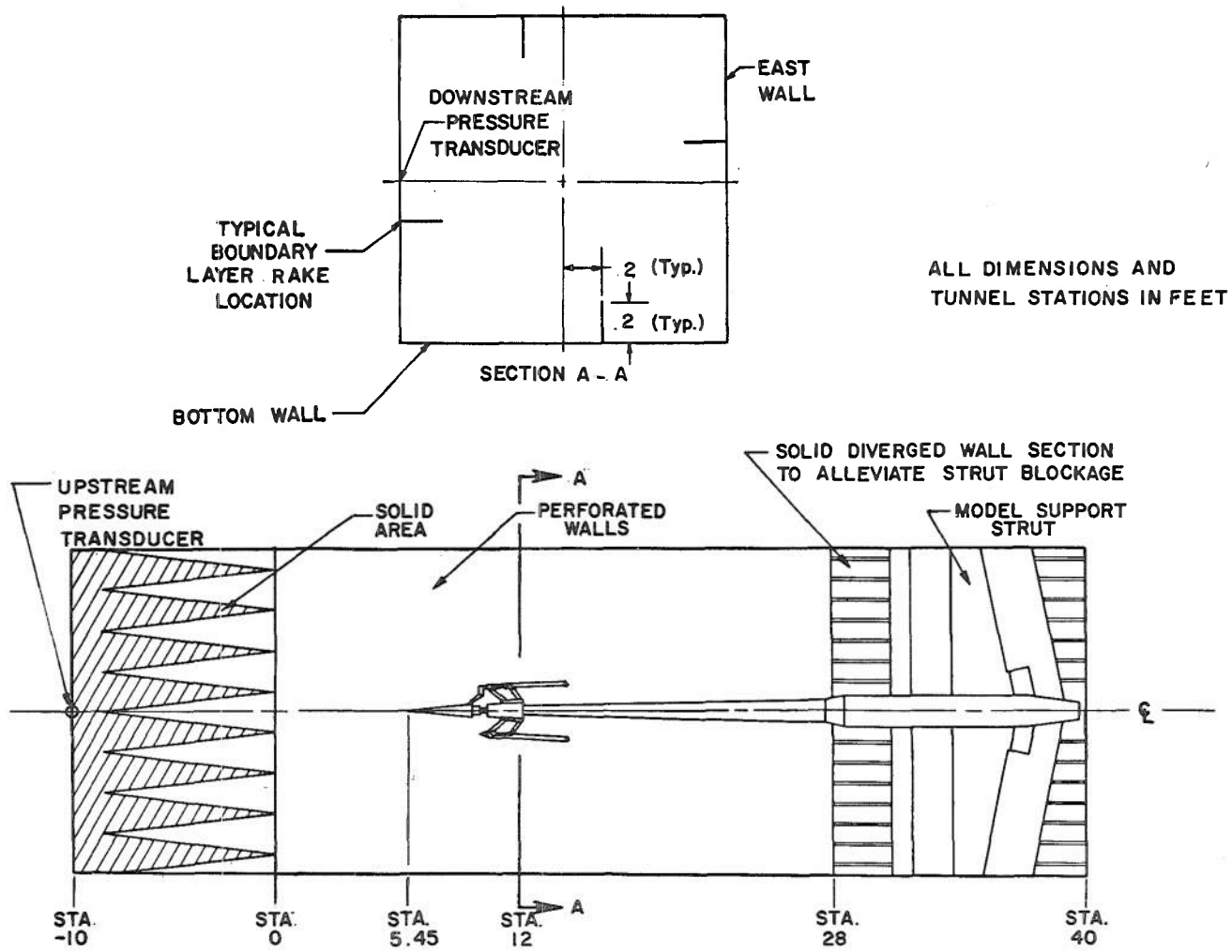

Fig. 1 Tunnel 16T Test Section with 10-deg Transition Cone and Wall Boundary-Layer Rakes Installed

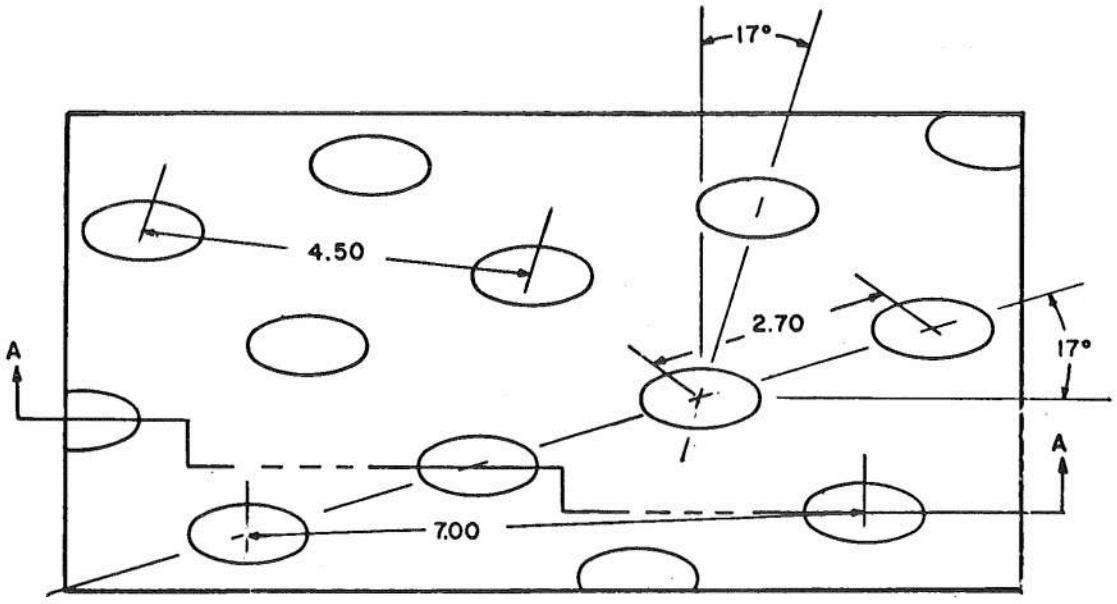

TYPICAL PERFORATED WALL PATTERN

ALL DIMENSIONS IN INCHES

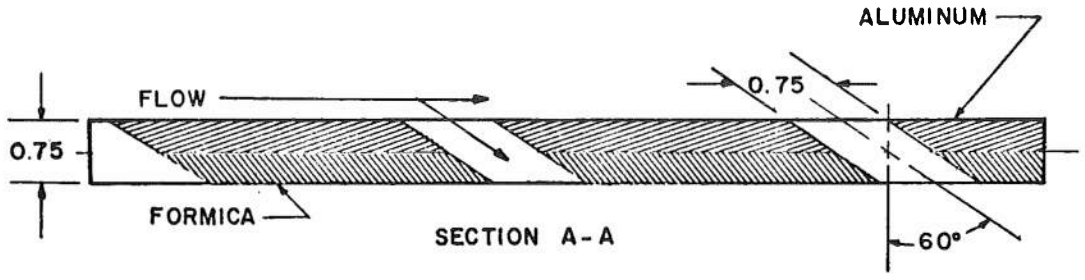

Fig. 2 Tunnel 16T Perforated Walls

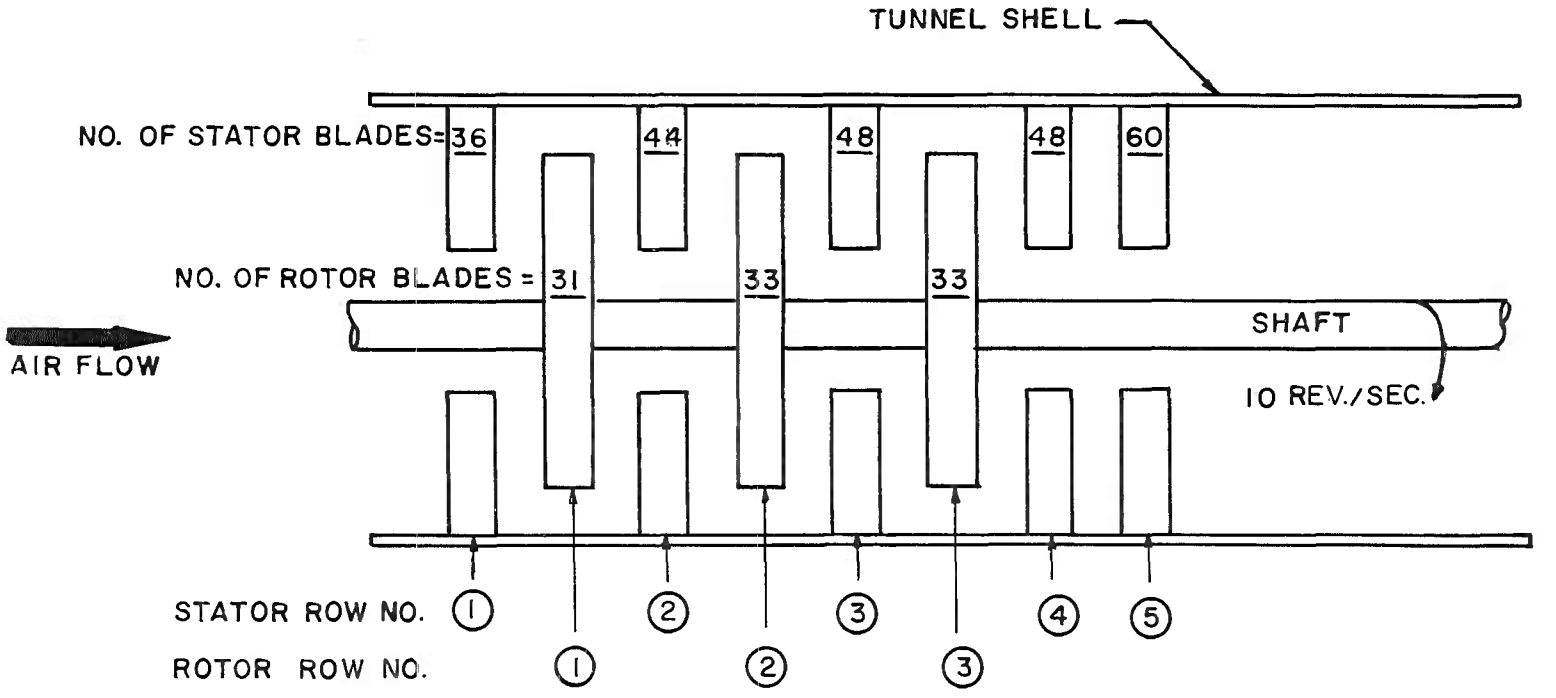

Fig. 3 Tunnel 16T Compressor

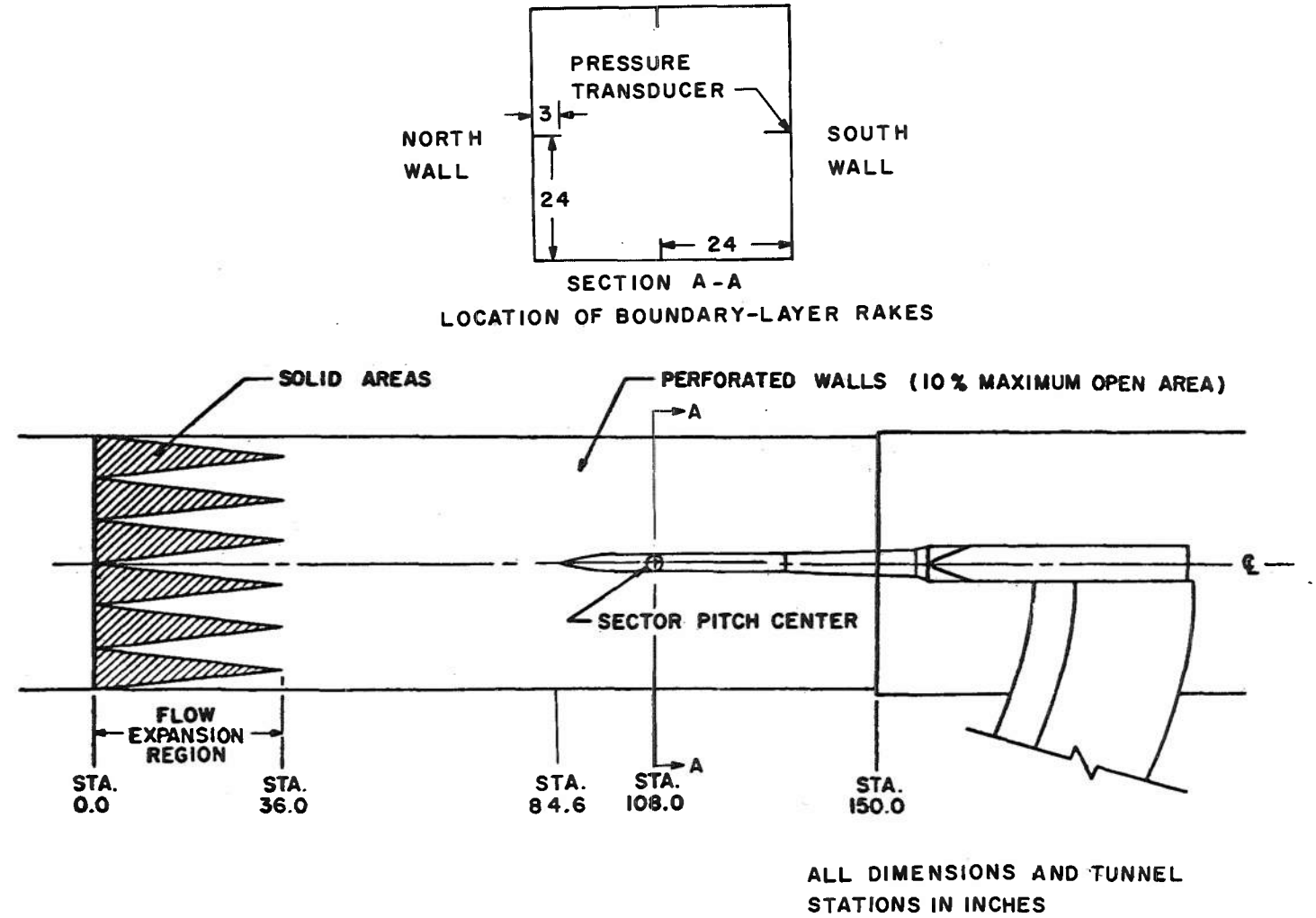

Fig. 4 Tunnel 4T Test Section with 2-in. Ogive Cylinder and Wall Boundary-Layer Rakes Installed

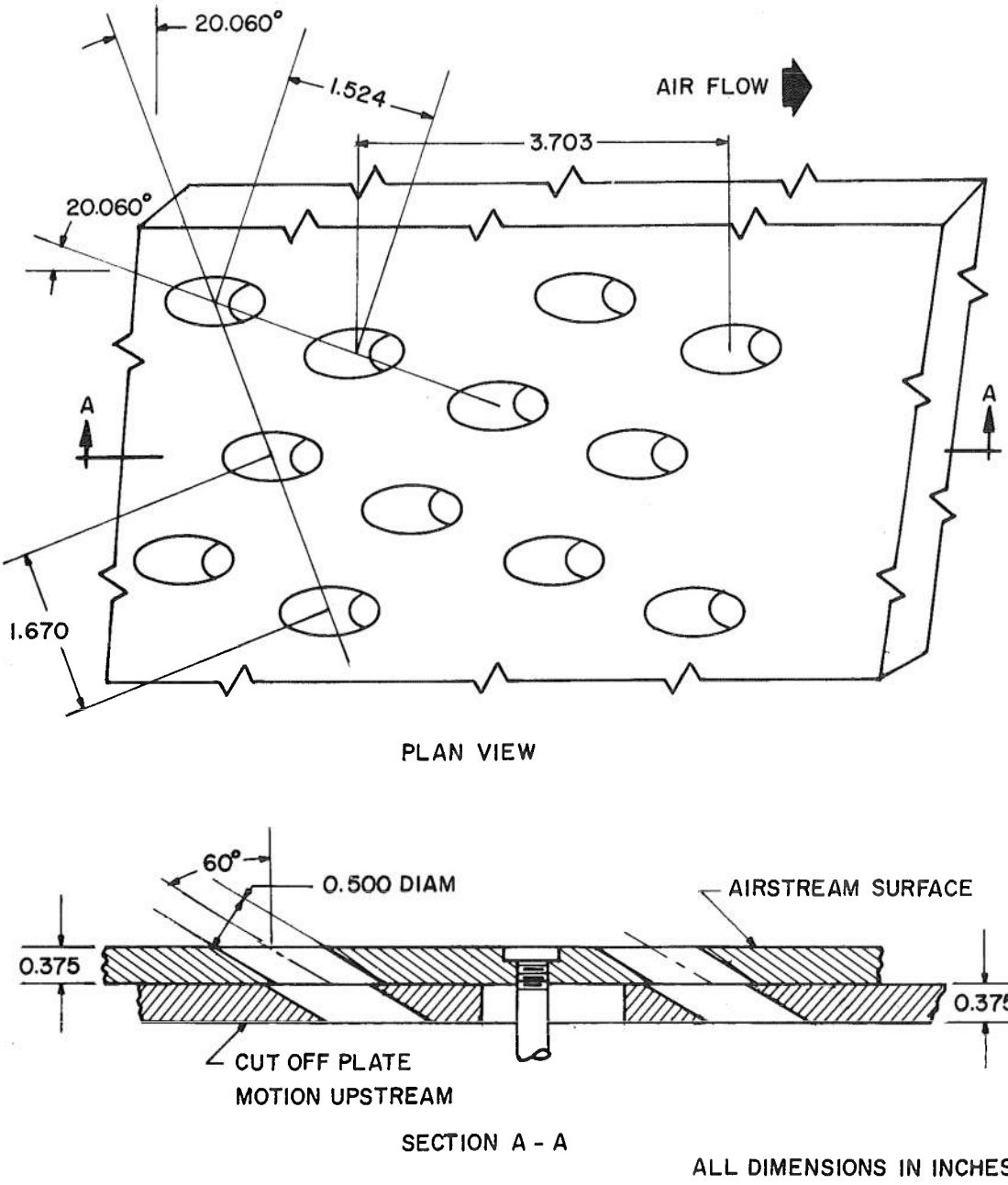

Fig. 5 Tunnel 4T Perforated Walls

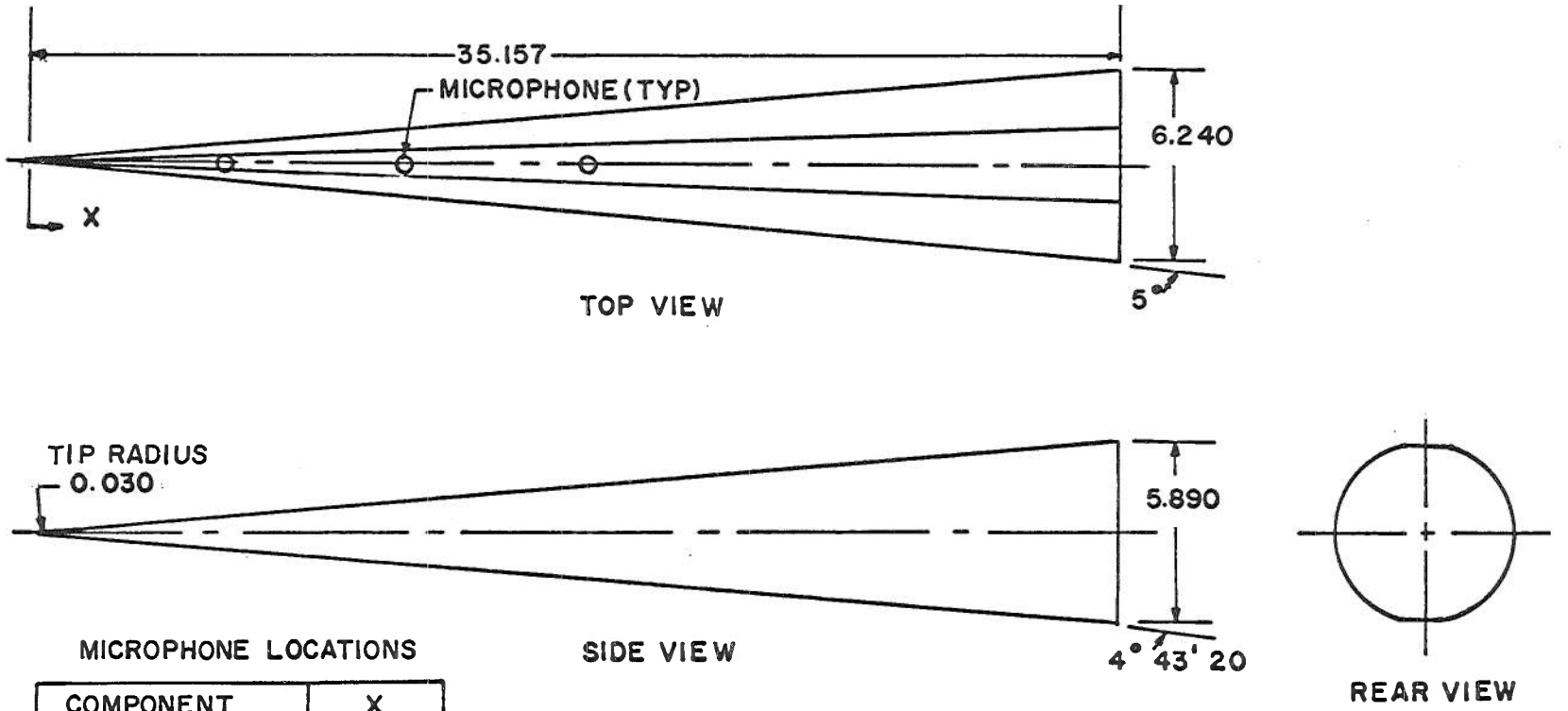

MICROPHONE LOCATIONS

COMPONENT	X
FORWARD MICROPHONE	5.741
CENTER MICROPHONE	11.350
AFT MICROPHONE	17.347

ALL DIMENSIONS IN INCHES

Fig. 6 Details of 10-deg Cone with Flats

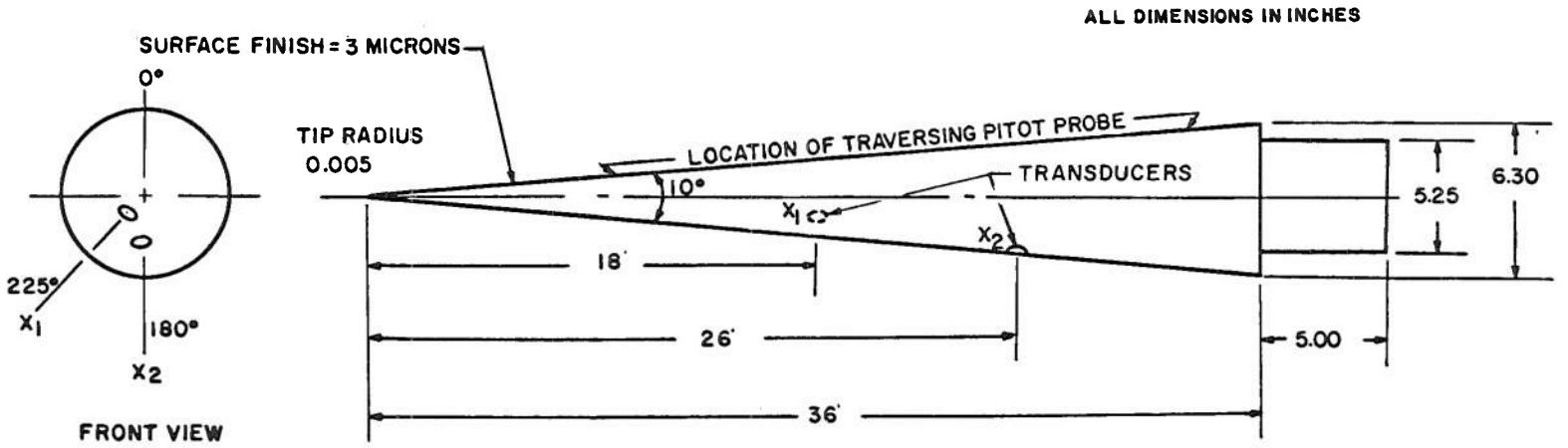

Fig. 7 Details of 10-deg Transition Cone

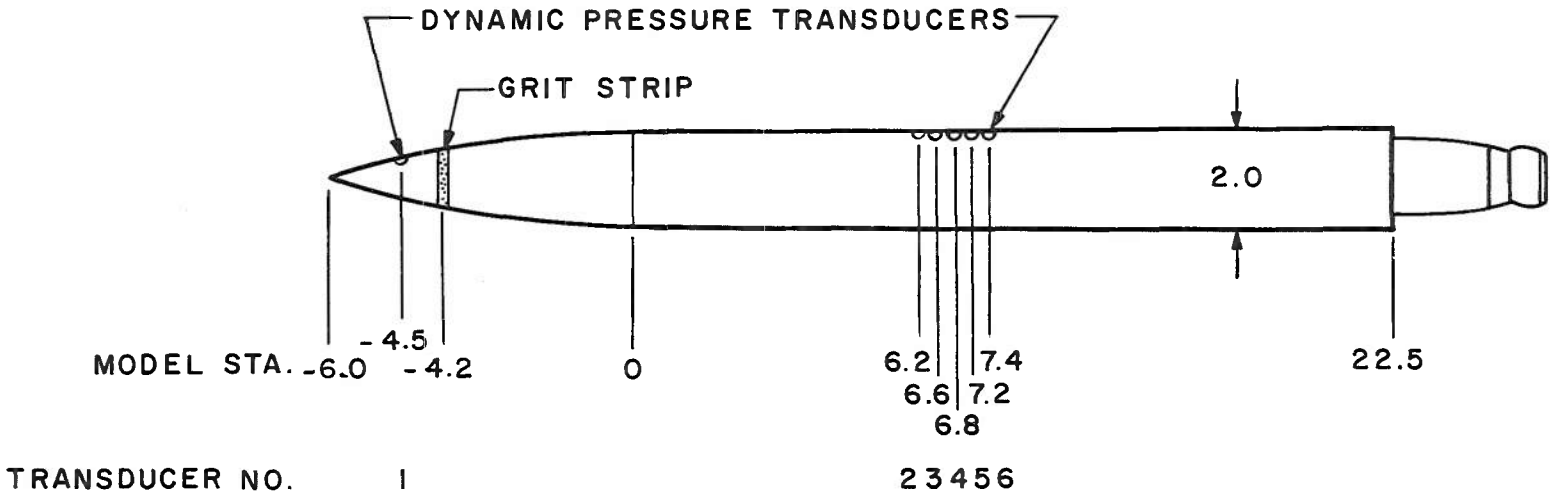

ALL DIMENSIONS IN INCHES

Fig. 8 Details of 2-in. Ogive Cylinder

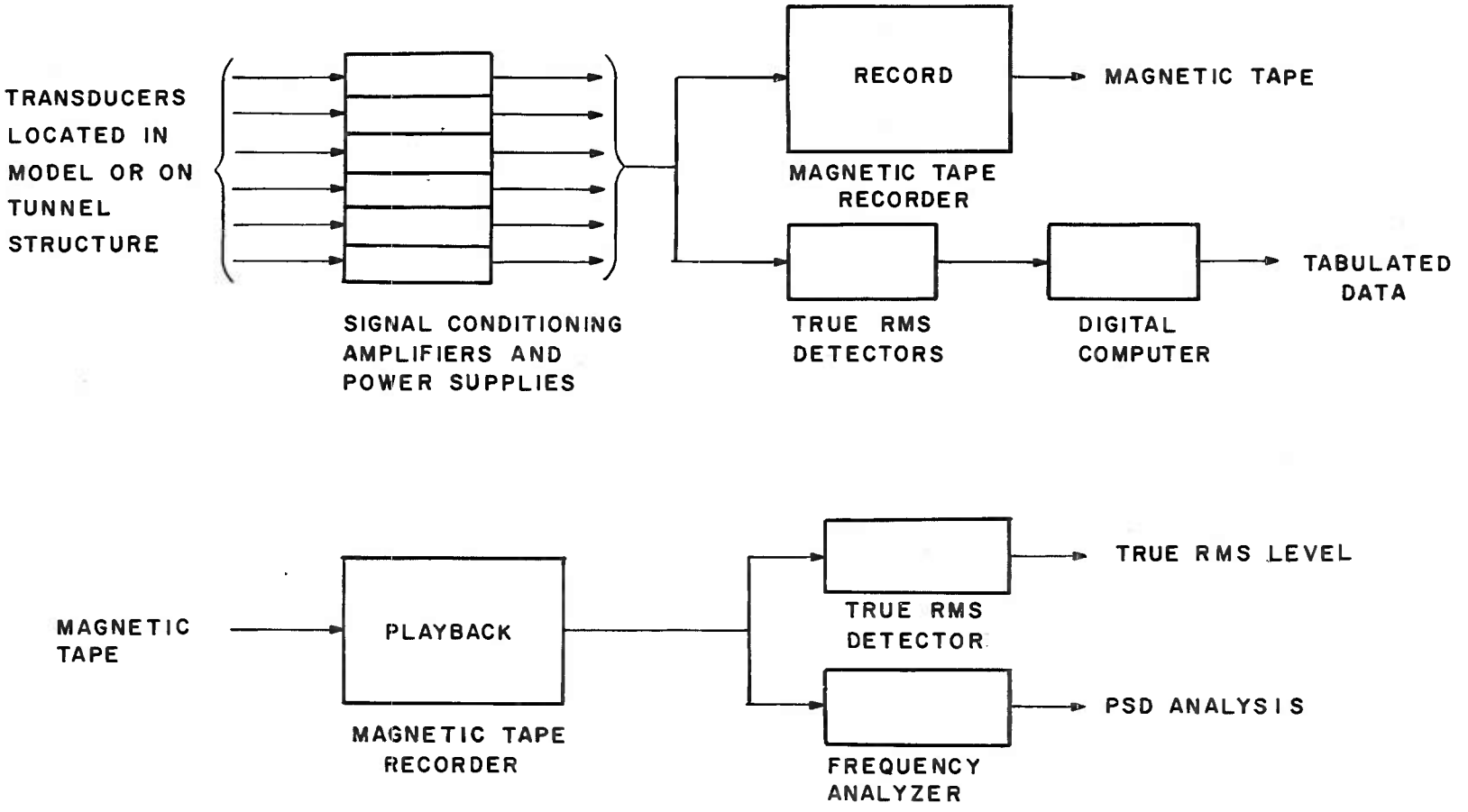

Fig. 9 Typical Instrumentation System for the Acquisition and Analysis of Data

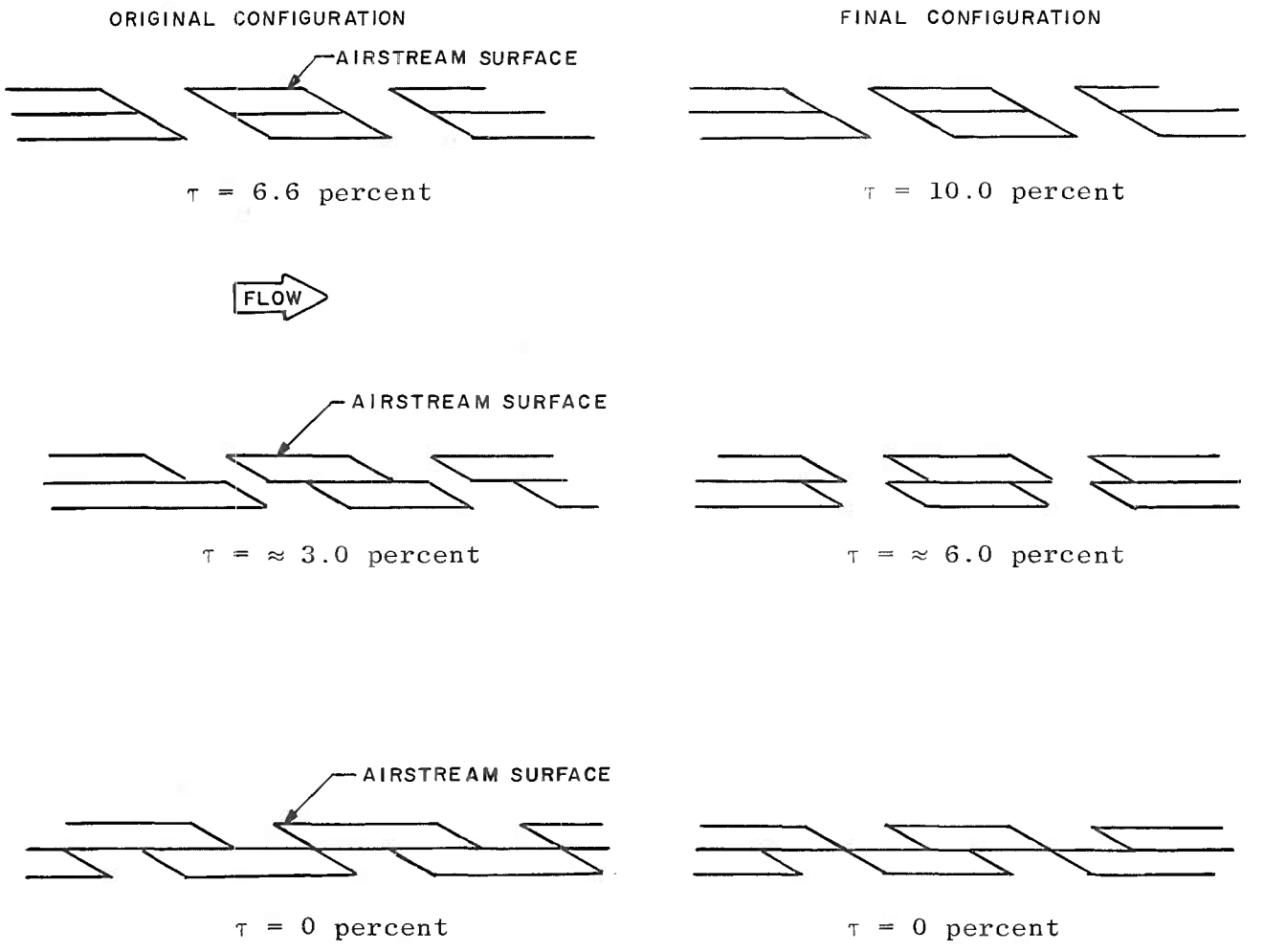

Fig. 10 Tunnel 4T Perforated Walls, Original and Final Configuration

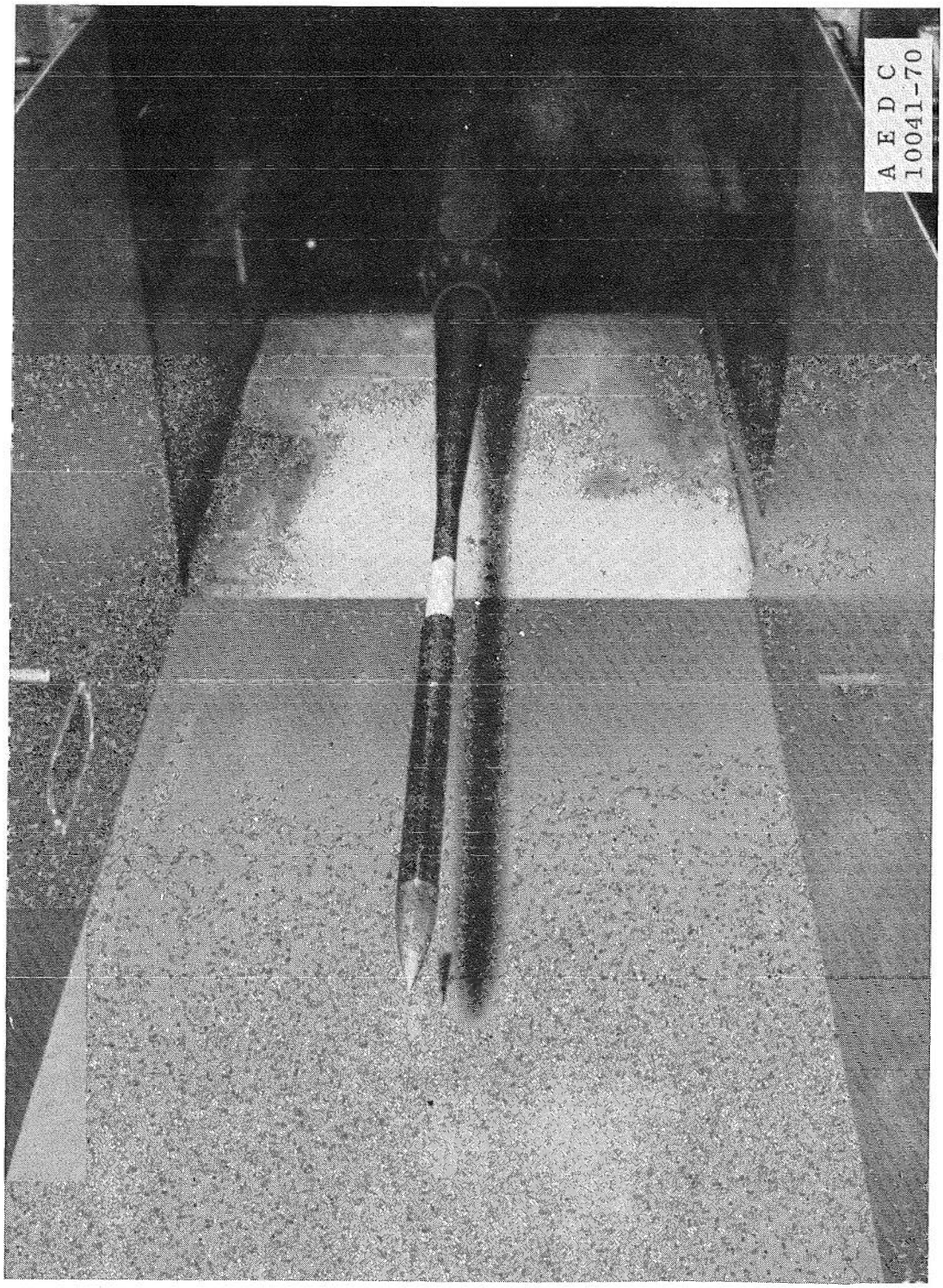

Fig. 11 Photograph of Taped Walls in Tunnel 4T with 2-in. Ogive Cylinder Installed

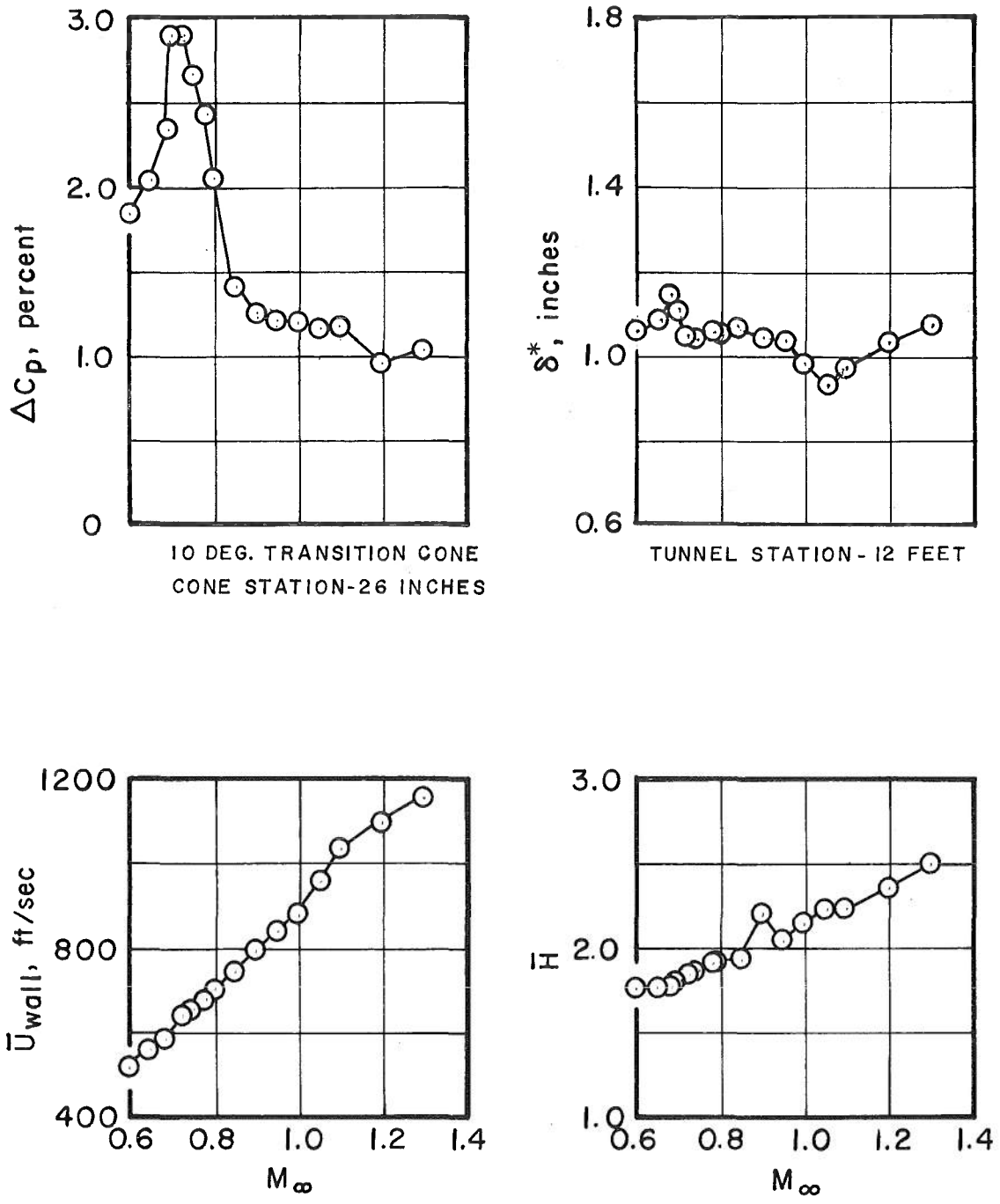

Fig. 12 Variation of Tunnel 16T Wall Boundary-Layer Characteristics and Test Section Noise Levels as a Function of Mach Number, p_t = 1185 psfa, θ_w = 0 deg

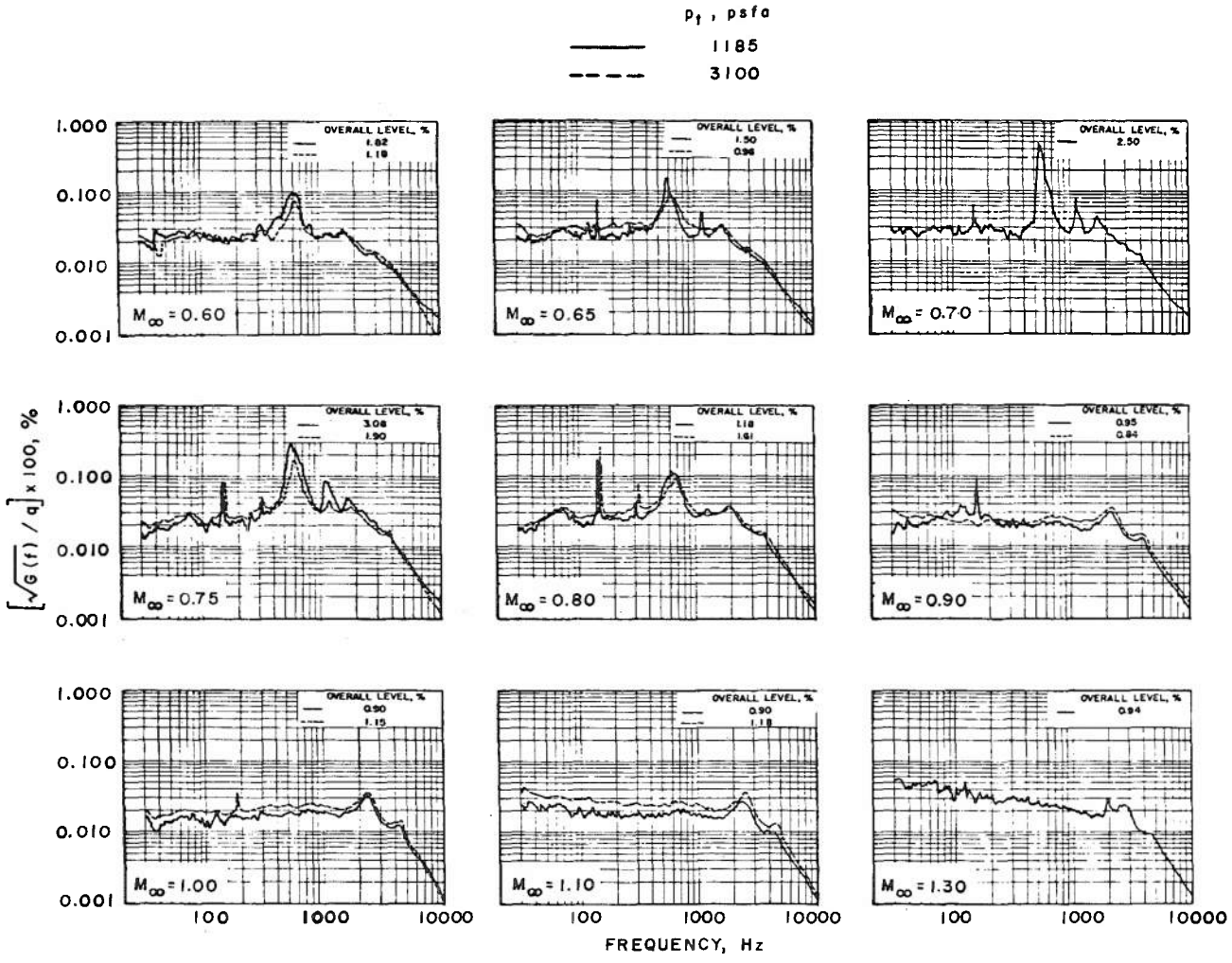

Fig. 13 Tunnel 16T Test Section Noise Spectra for Various Mach Numbers, 10-deg Cone with Flats, Cone Station 5.71 in., θ_w = 0 deg, p_t = 1185 and 3100 psfa

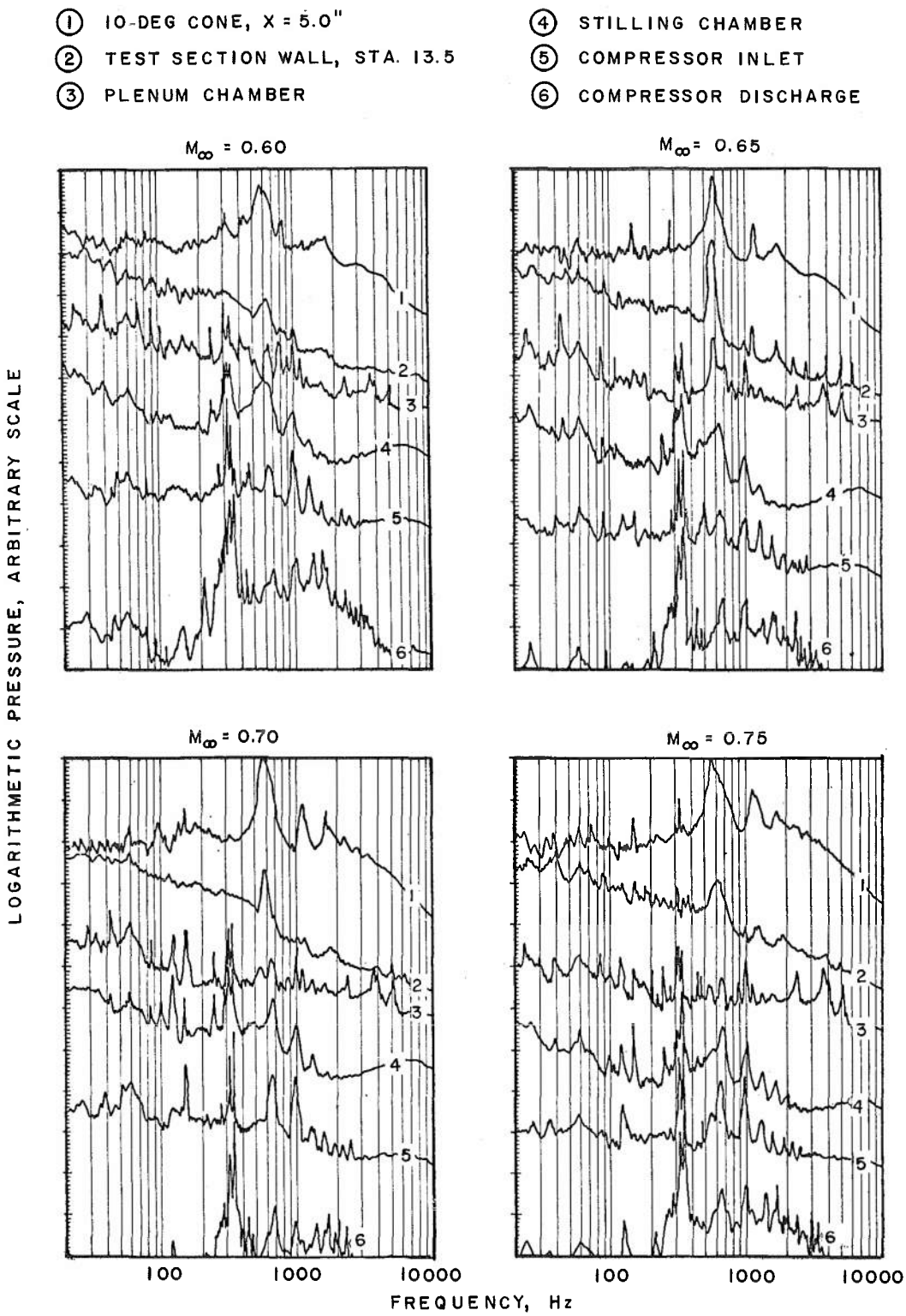

a. M_∞ = 0.60 to 0.75

Fig. 14 Comparison of Tunnel 16T Frequency Spectra Measured around the Tunnel Circuit, p_t = 1185 psfa

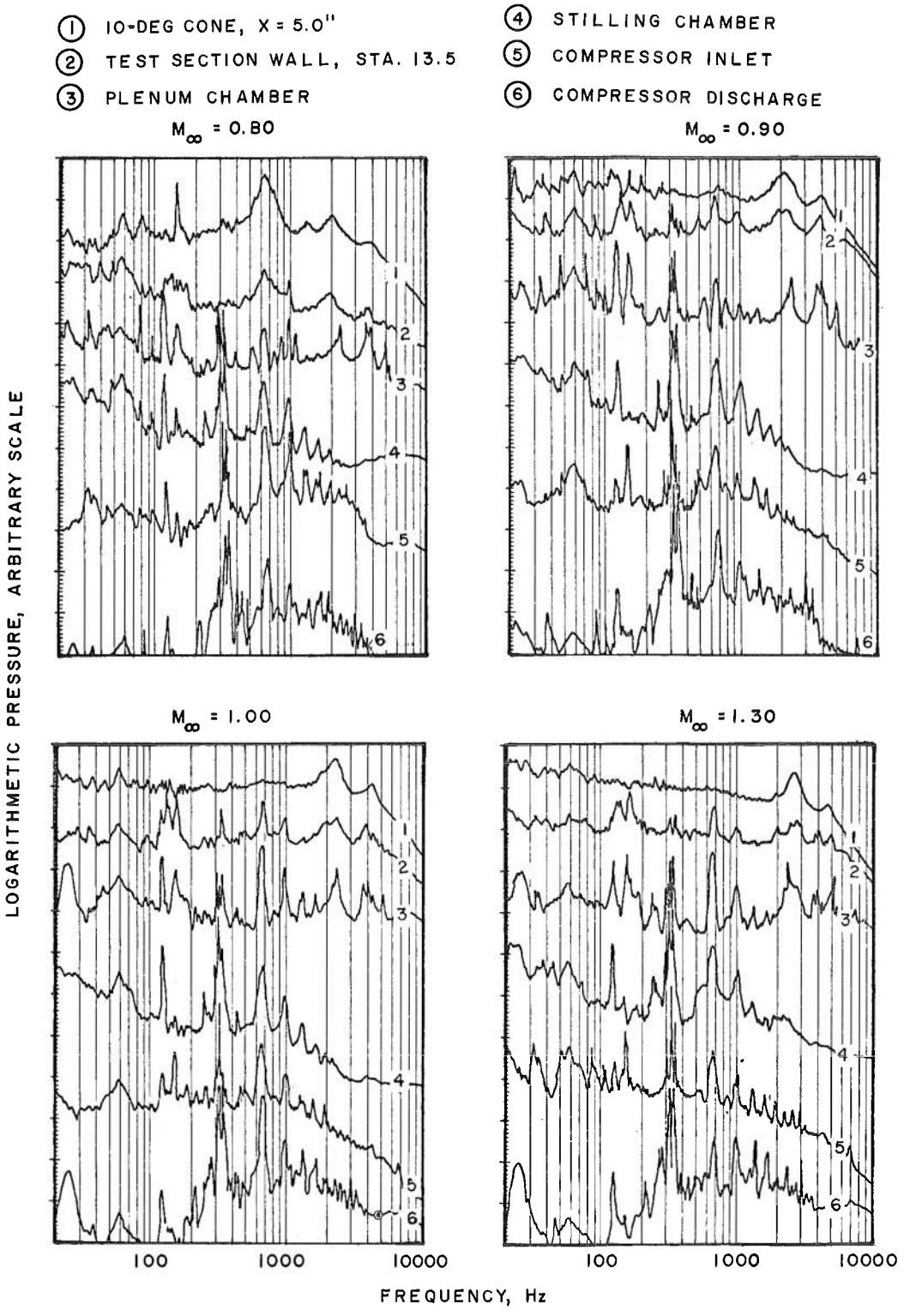

b. M_∞ = 0.80 to 1.30
Fig. 14 Concluded

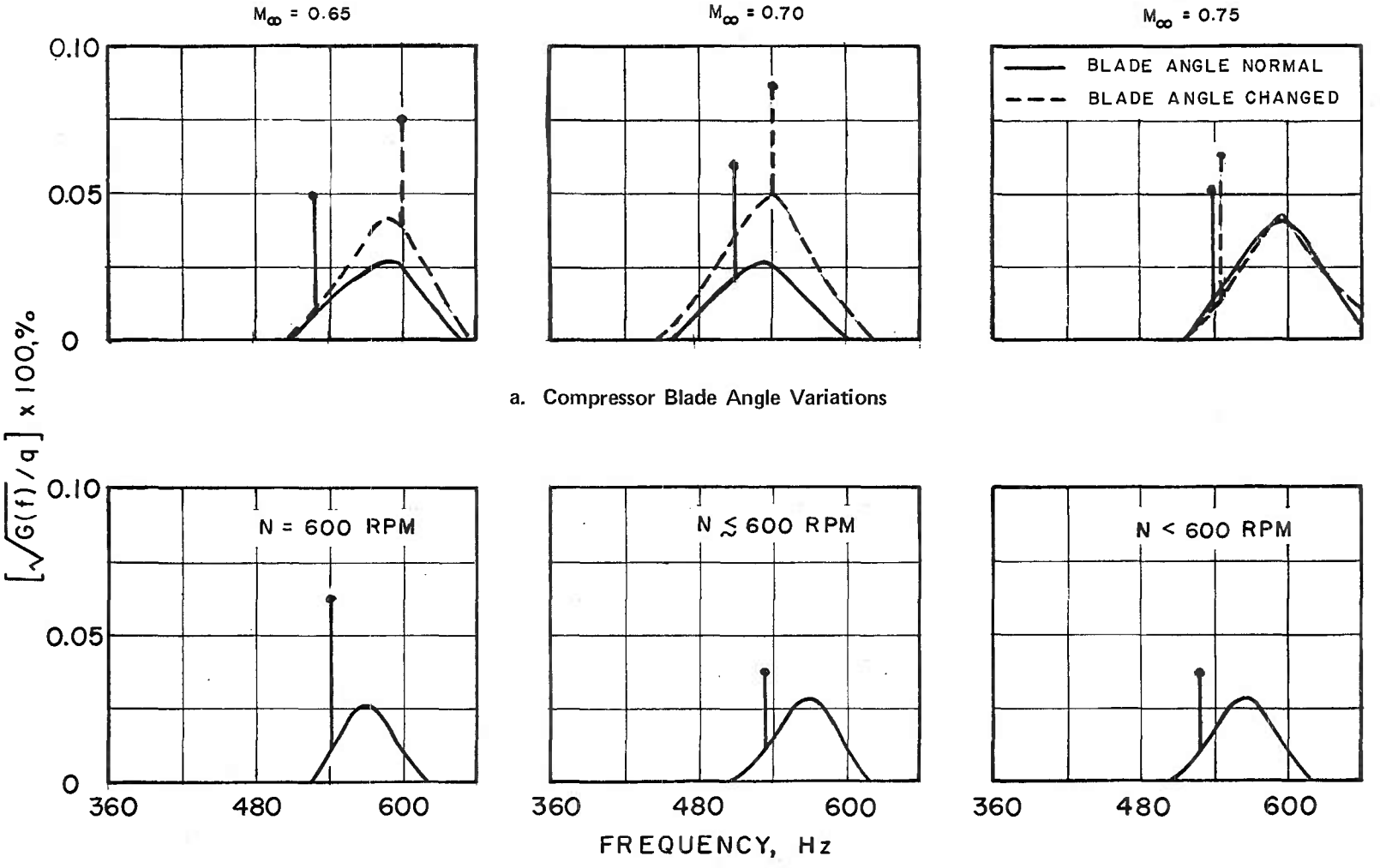

a. Compressor Blade Angle Variations

b. Compressor Coast Down, M_∞ = 0.75

Fig. 15 Evaluation of the Influence of the Tunnel 16T Compressor Operating Conditions on the Test Section Noise Spectra, p_t = 1185 psfa

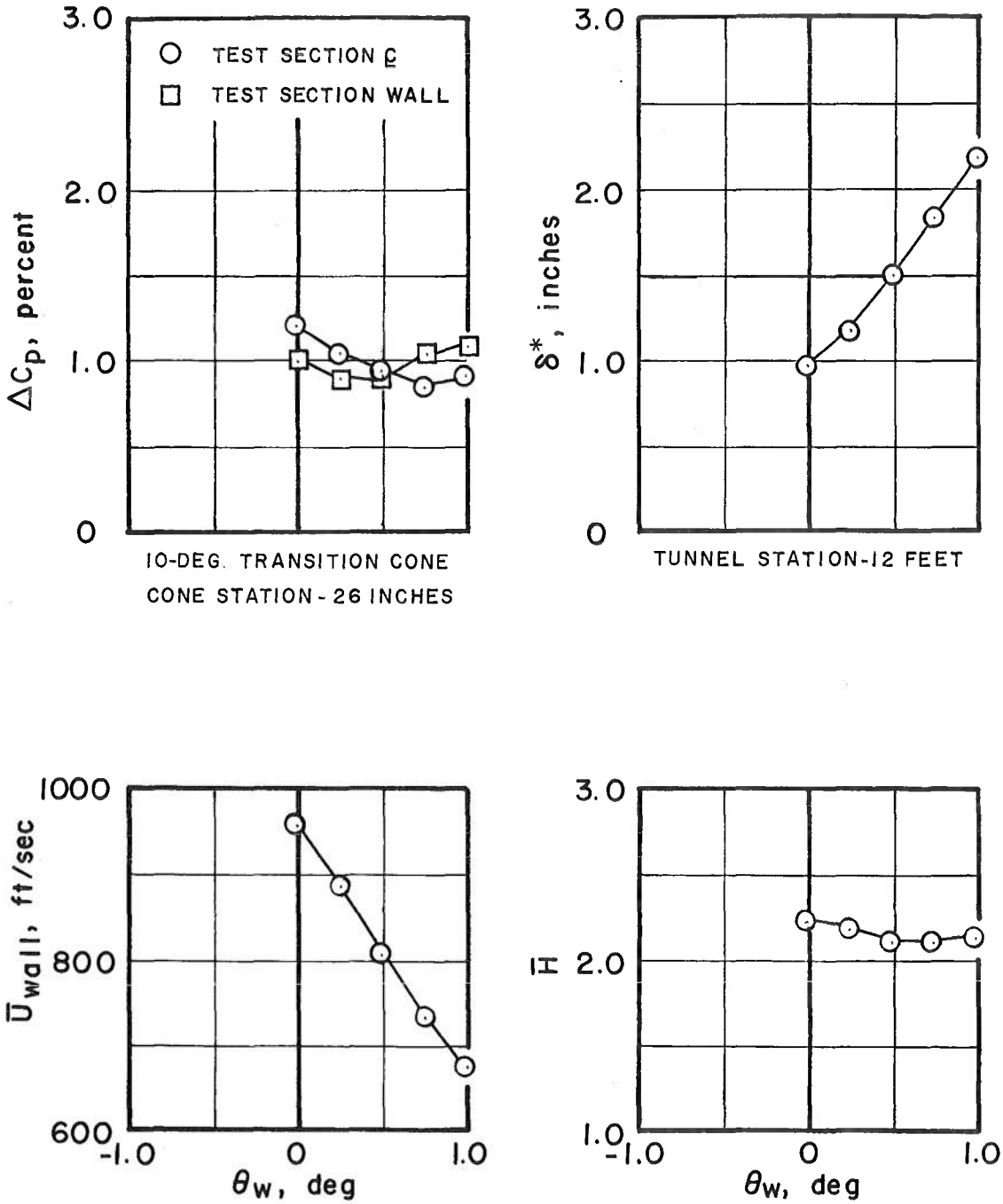

a. $M_\infty = 1.05$

Fig. 16 Variations of Tunnel 16T Wall Boundary-Layer Characteristics and Test Section Noise Levels as a Function of Wall Angle, p_t = 1185 psfa

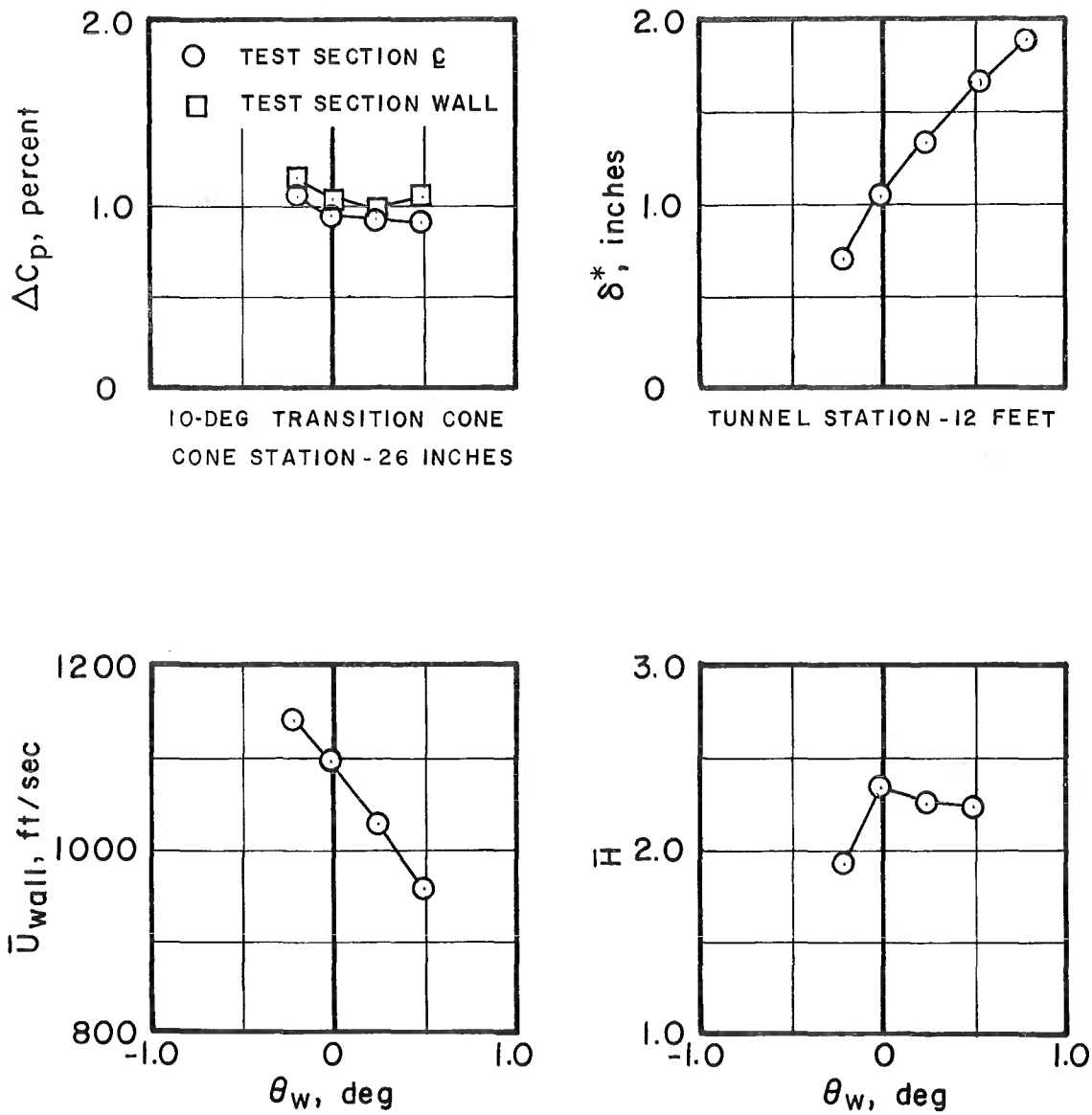

b. $M_\infty = 1.20$

Fig. 16 Concluded

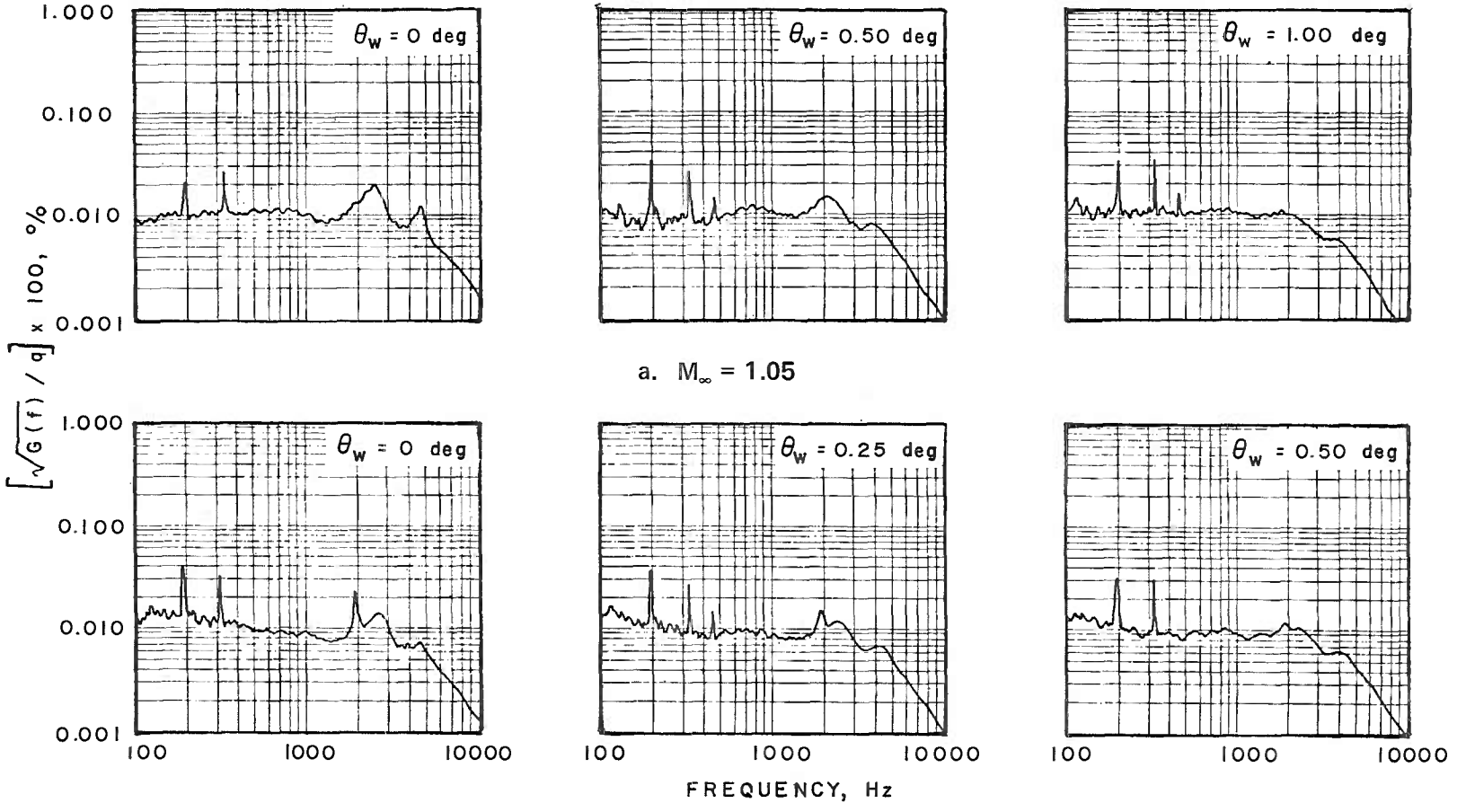

b. M_∞ = 1.20

Fig. 17 Comparison of Tunnel 16T Test Section Noise Spectra for Various Wall Angles, 10-deg Transition Cone, Cone Station 26 in., p_t = 1185 psfa

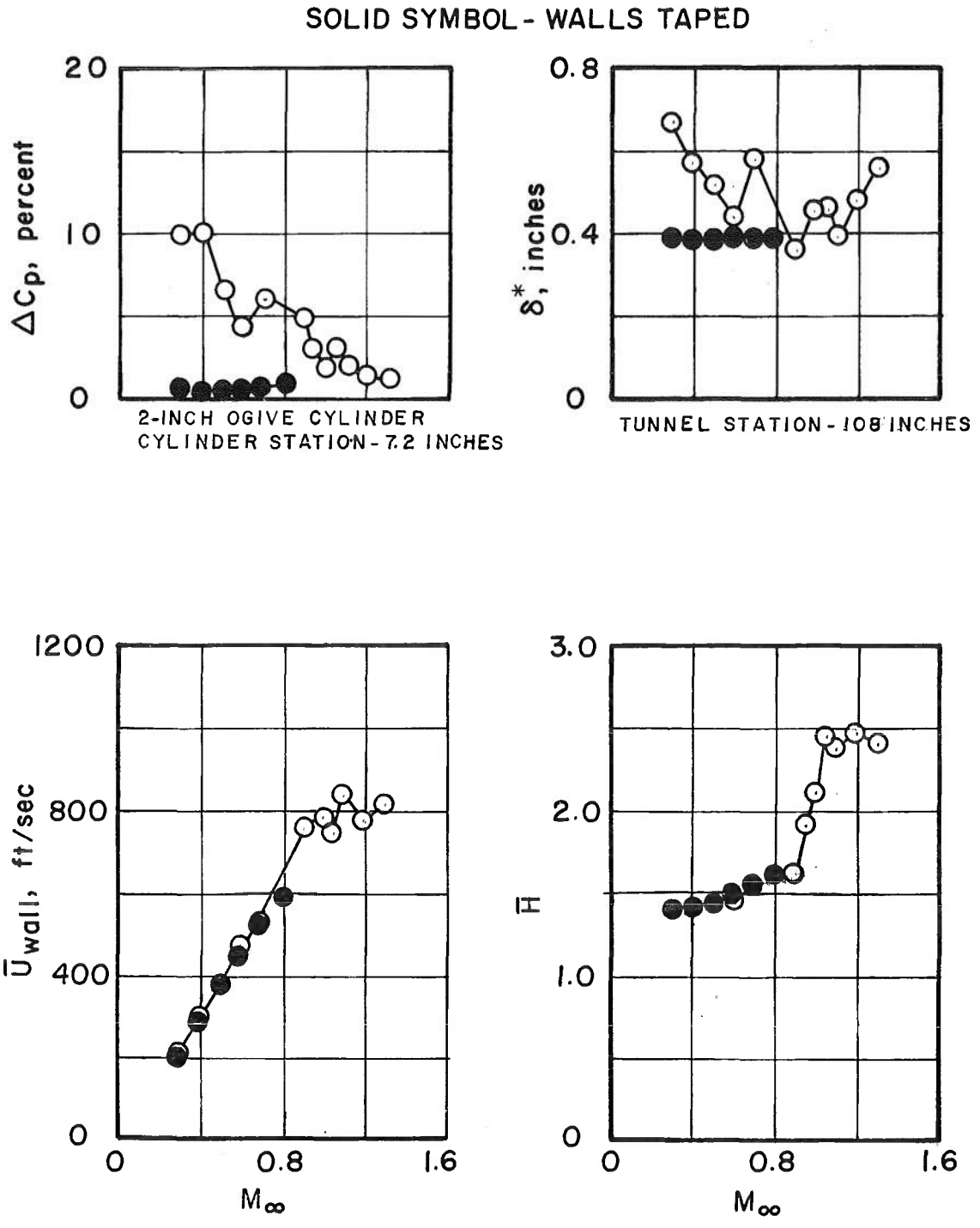

a. τ = 10 percent

Fig. 18 Variation of Tunnel 4T Wall Boundary-Layer Characteristics and Test Section Noise Levels as a Function of Mach Number, p_t = 1185 psfa, θ_w = 0 deg

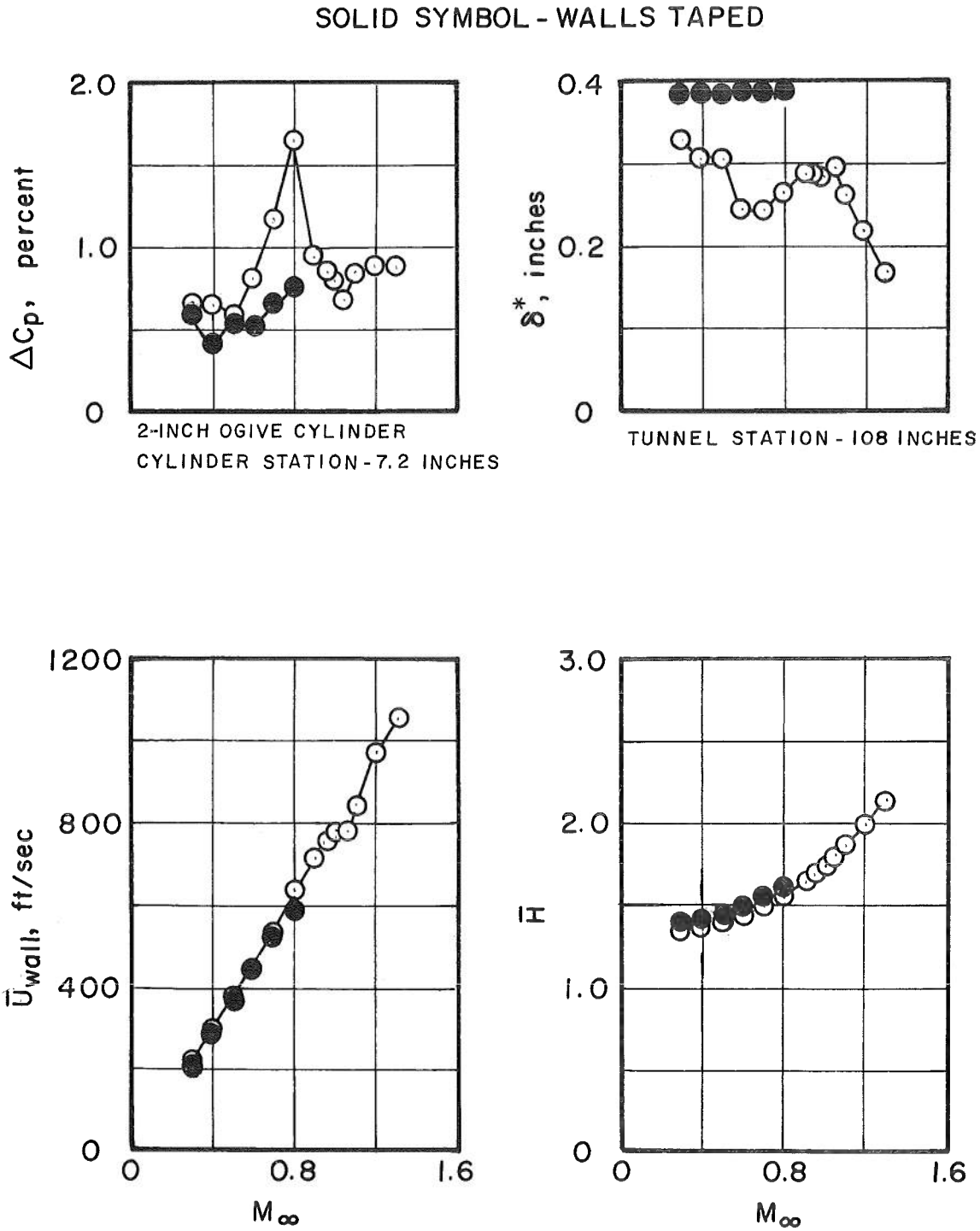

b. τ = 6 percent
Fig. 18 Continued

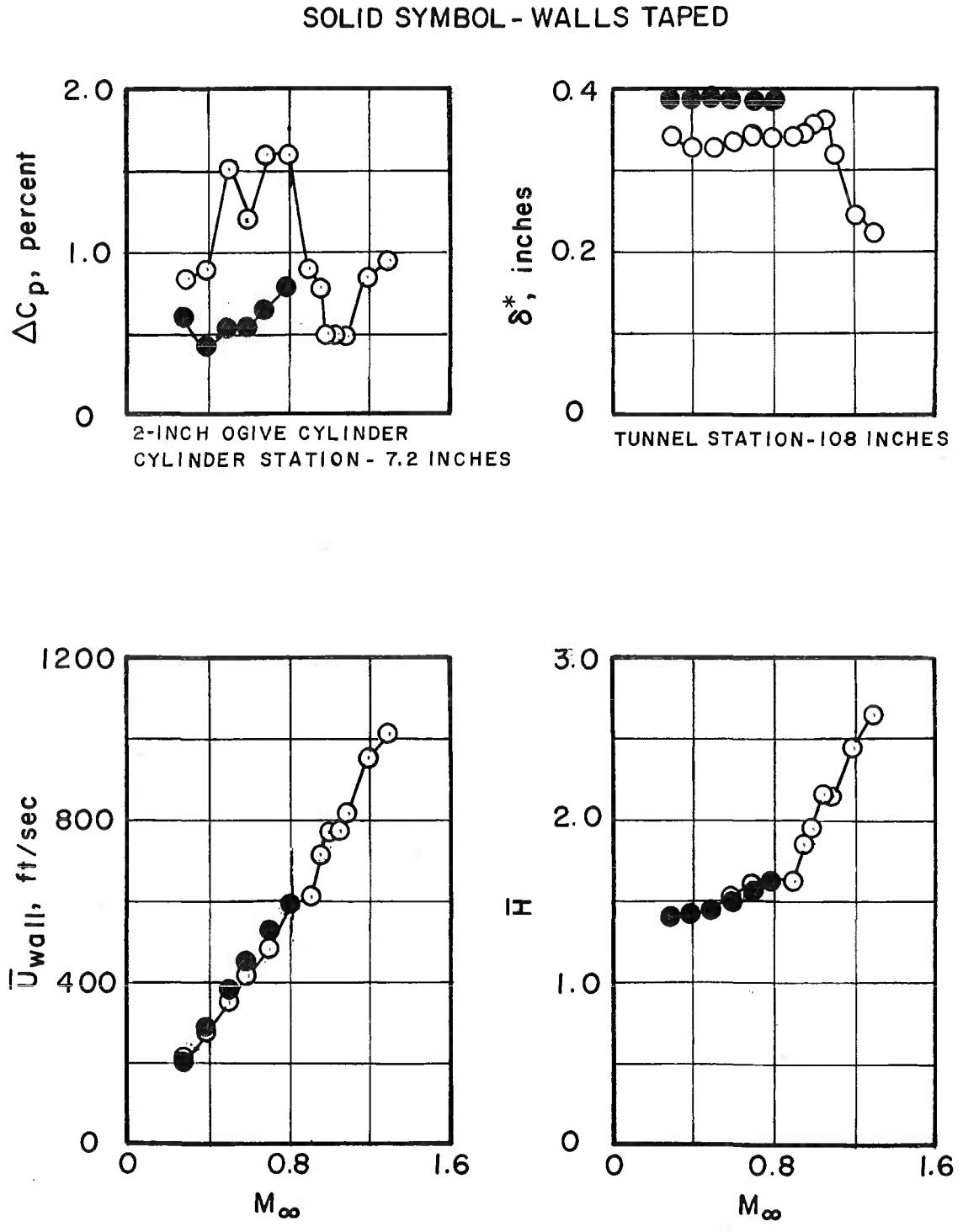

c. τ = Optimum

Fig. 18 Concluded

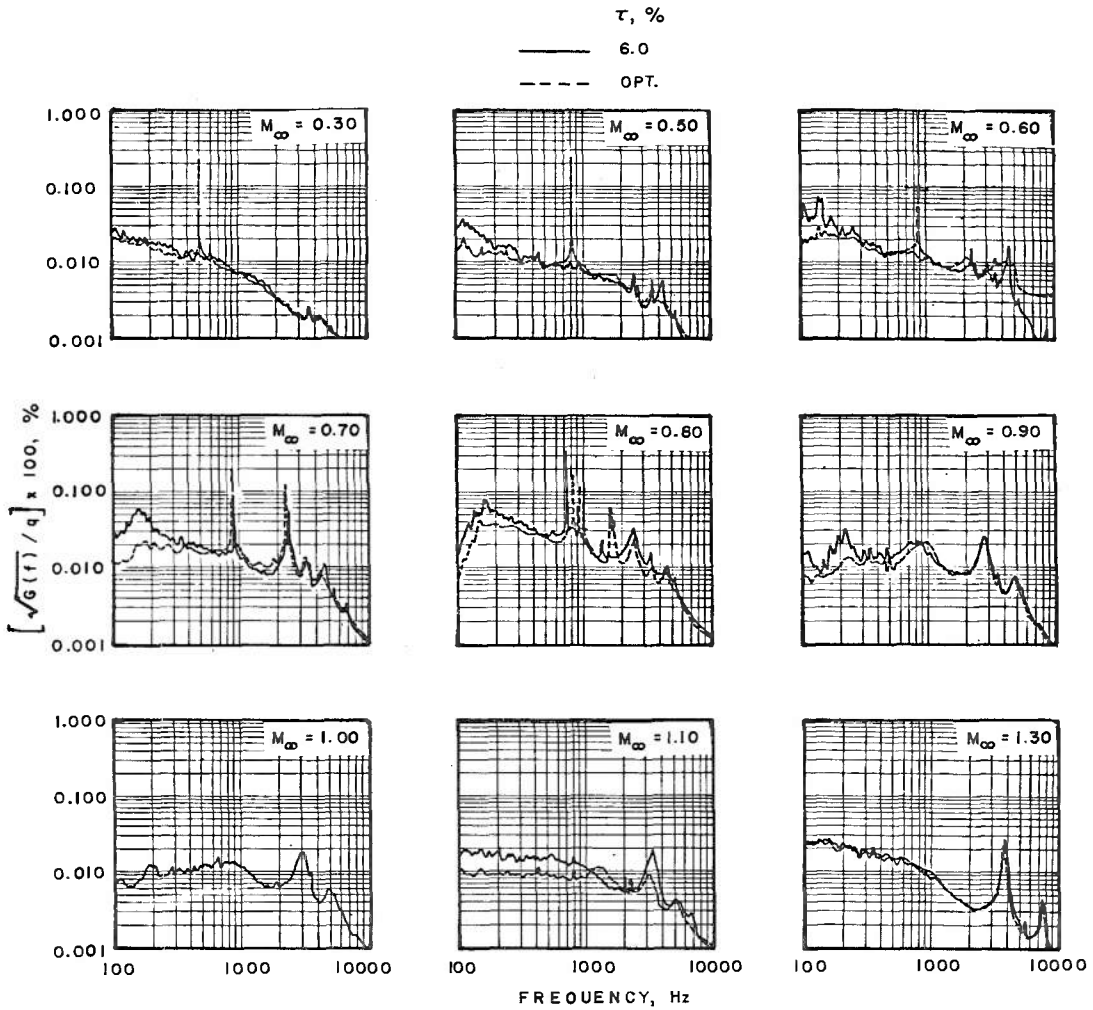

Fig. 19 Tunnel 4T Test Section Noise Spectra for Various Mach Numbers, 2-in. Ogive Cylinder, Cylinder Station 7.2 in., p_t = 1185 psfa, θ_{vv} = 0 deg

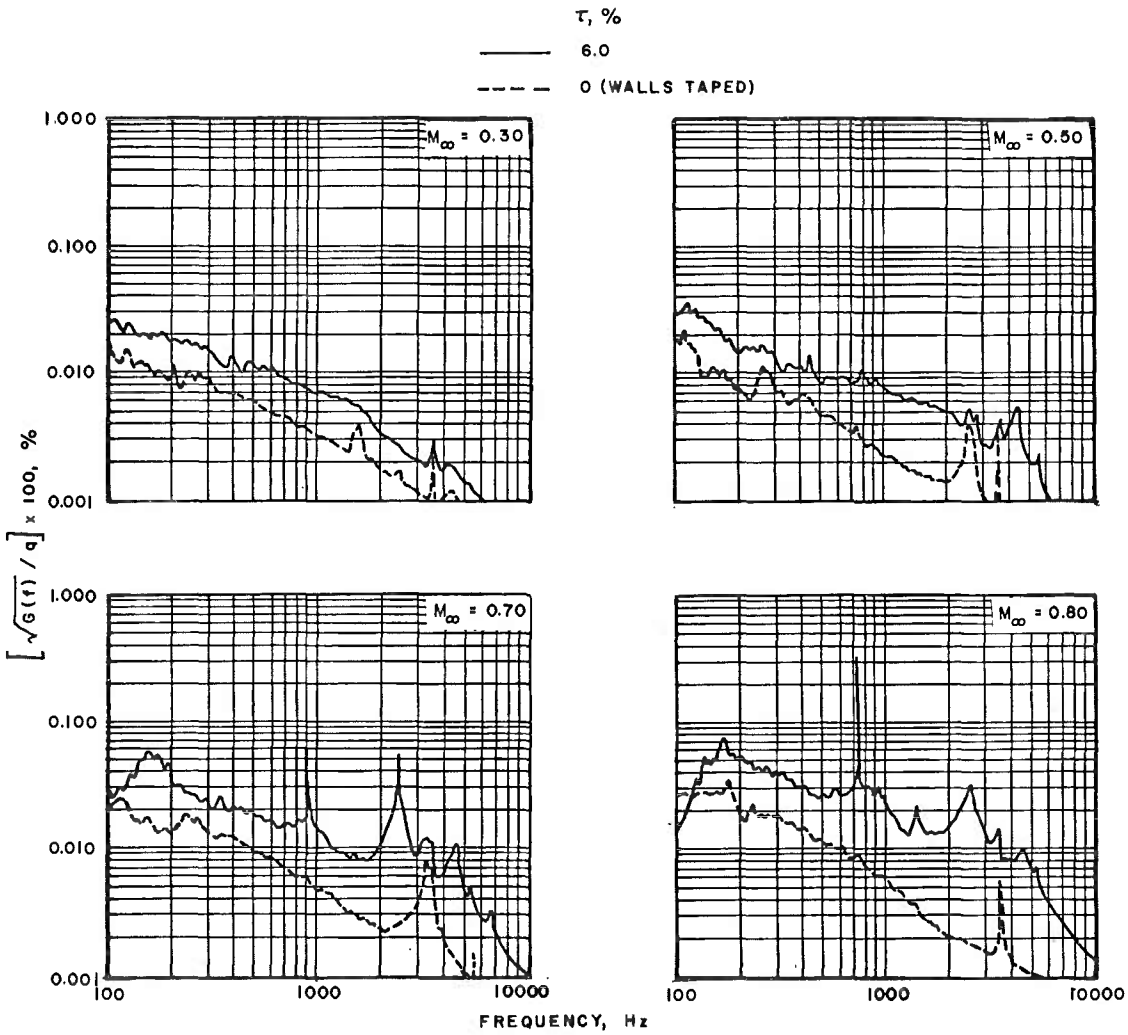

Fig. 20 Comparison of Tunnel 4T Test Section Noise Spectra with Open and Taped Walls, p_t = 1185 psfa

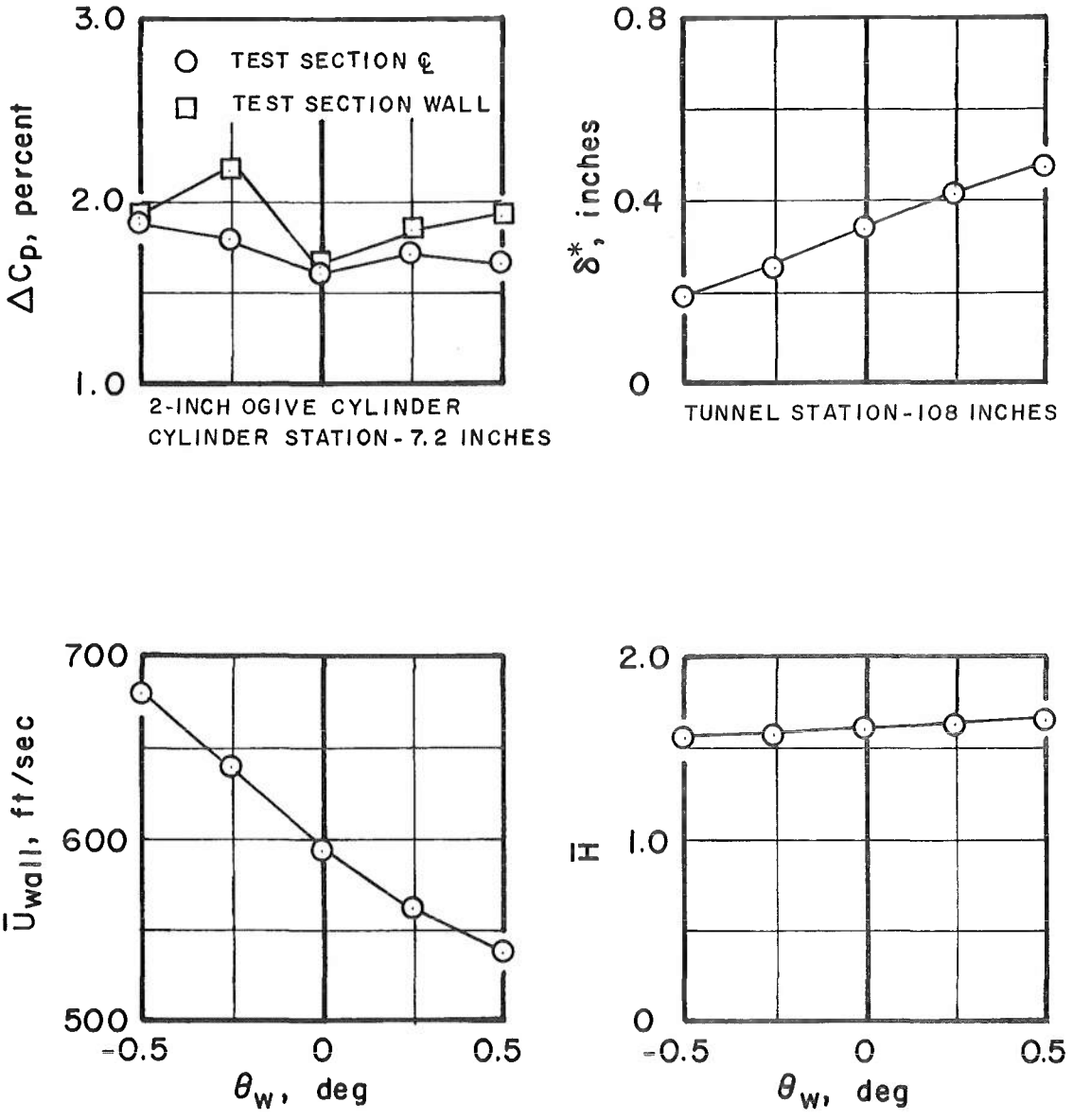

a. $M_\infty = 0.80$, $\tau = 5.00$ percent

Fig. 21 Variations of Tunnel 4T Wall Boundary-Layer Characteristics and Overall Test Section Noise Levels as a Function of Wall Angle, $p_t = 1185$ psfa

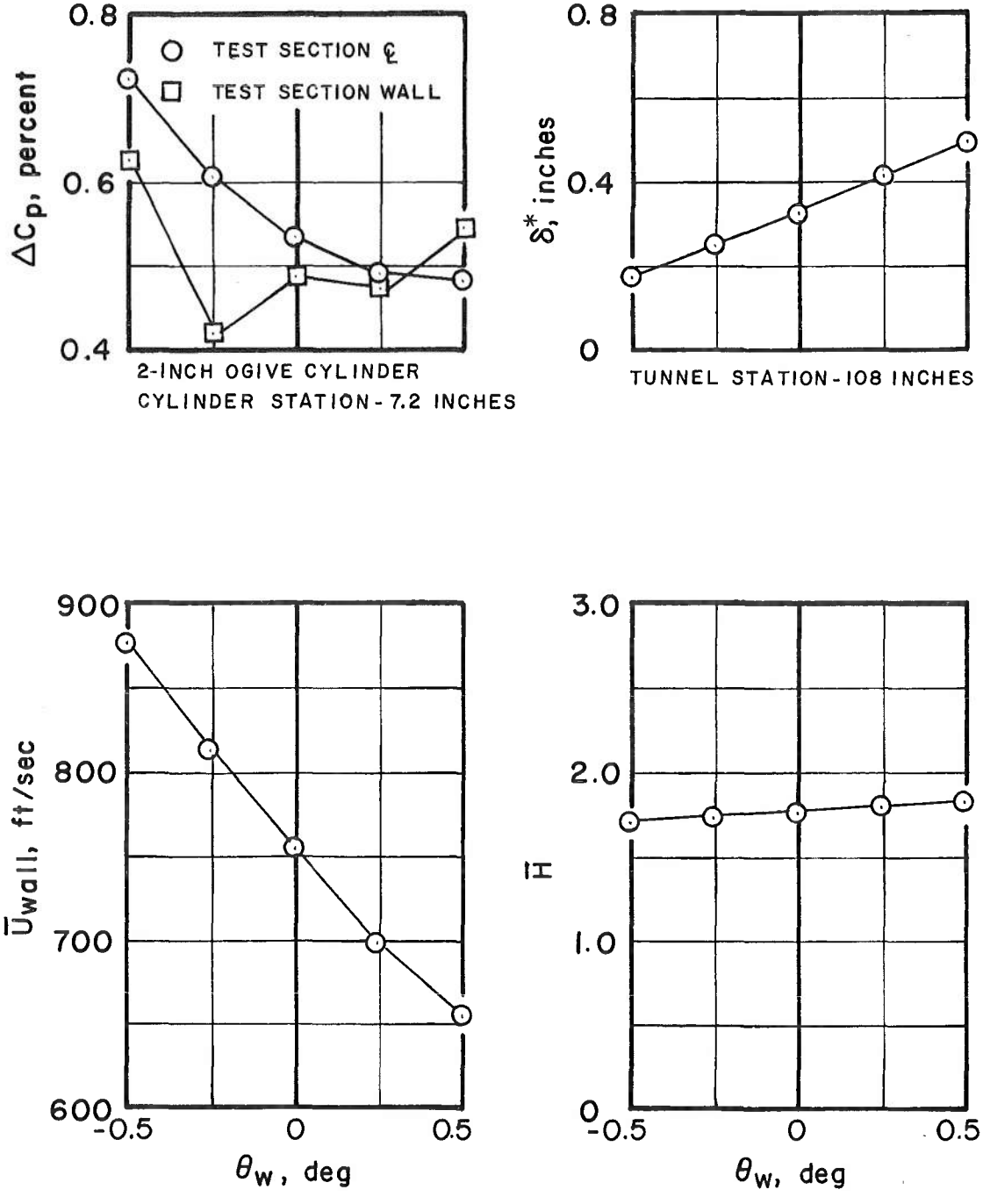

b. M_∞ = 1.00, τ = 1.44 percent
Fig. 21 Continued

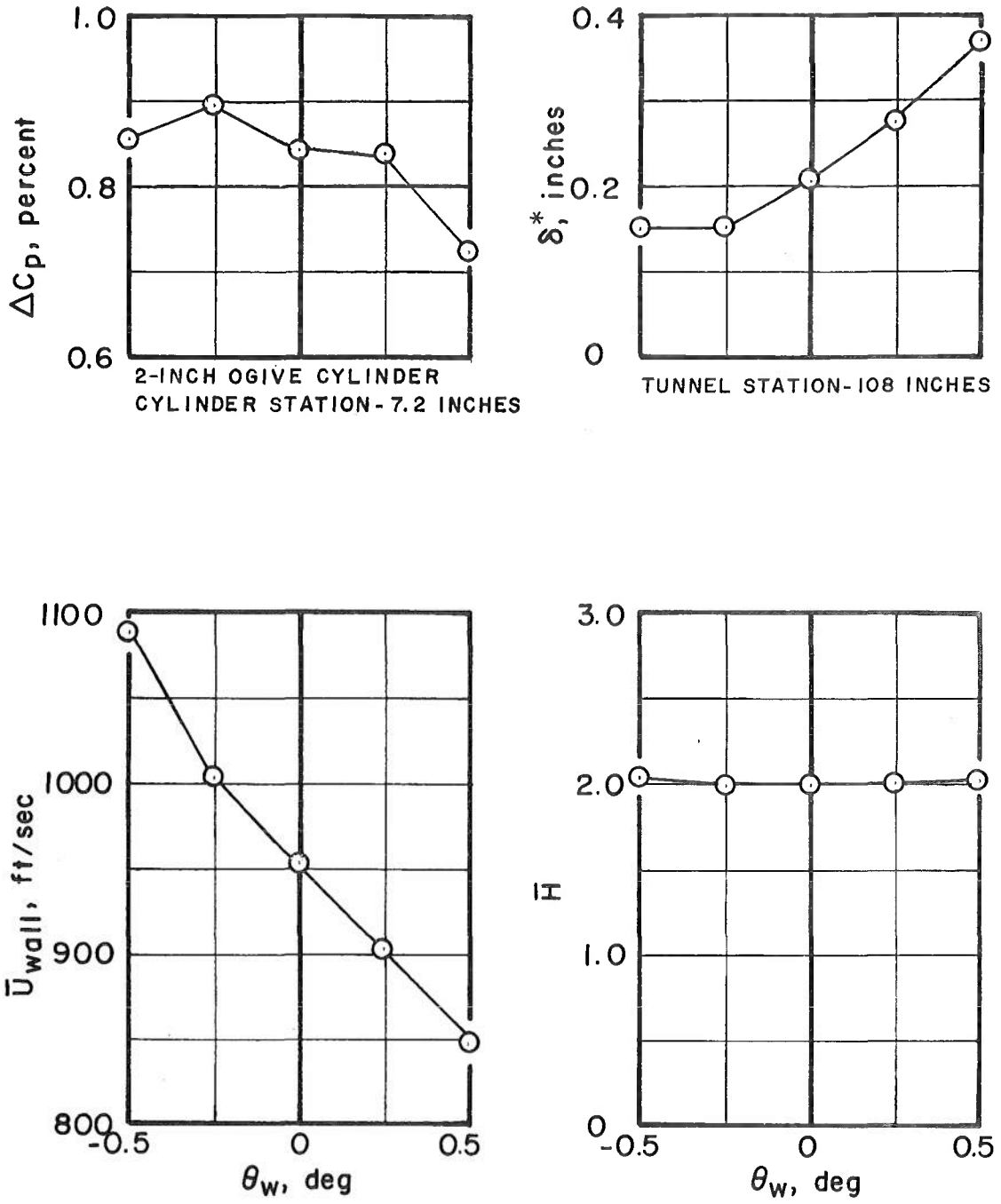

c. M_∞ = 1.20, τ = 4.72 percent
Fig. 21 Concluded

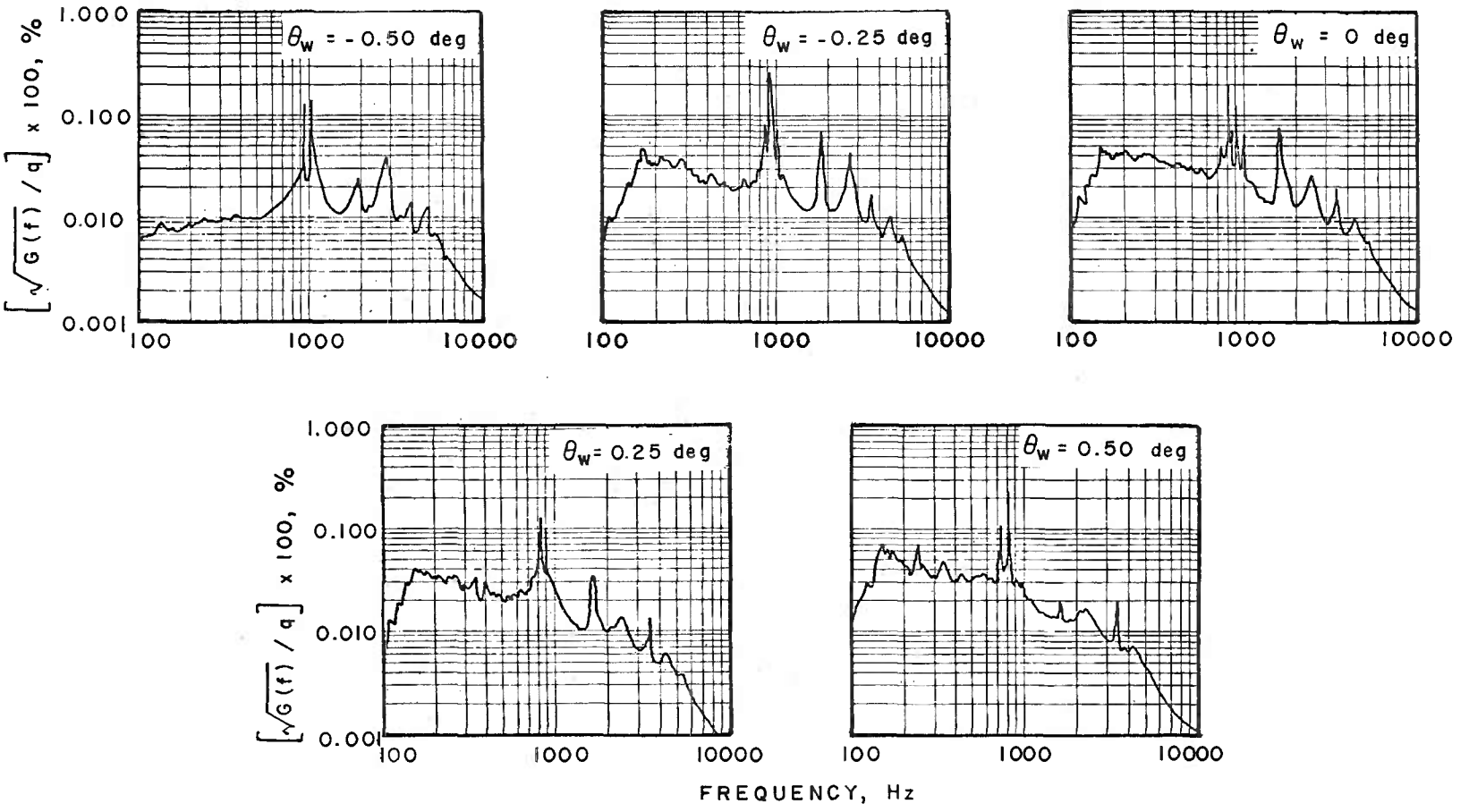

a. M_∞ = 0.80, τ = 5.00 percent

Fig. 22 Tunnel 4T Test Section Noise Spectra for Various Wall Angles, 2-in. Ogive Cylinder, Cylinder Station 7.2 in., p_t = 1185 psfa

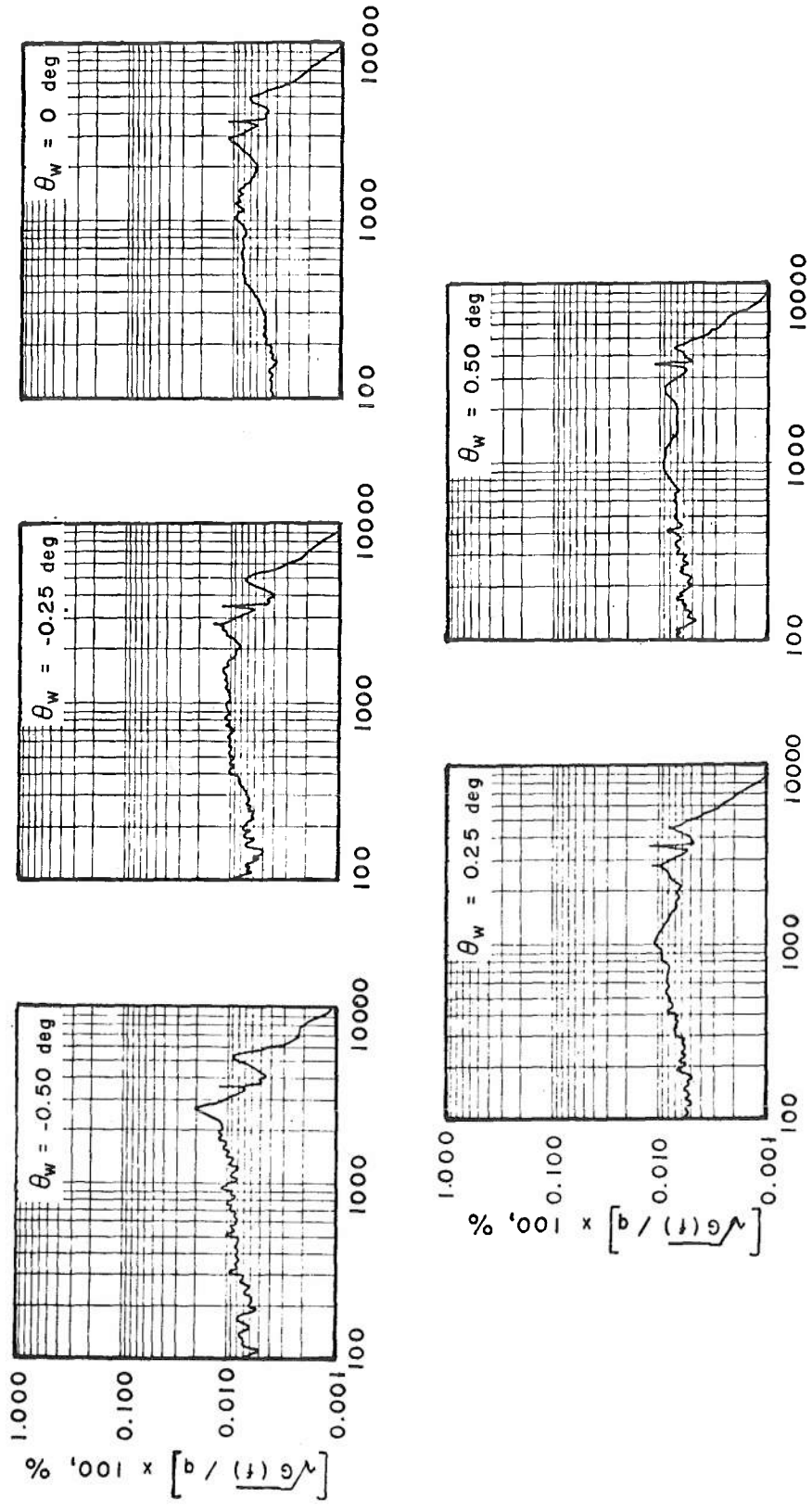

b. $M_\infty = 1.00$, $\tau = 1.44$ percent
Fig. 22 Concluded

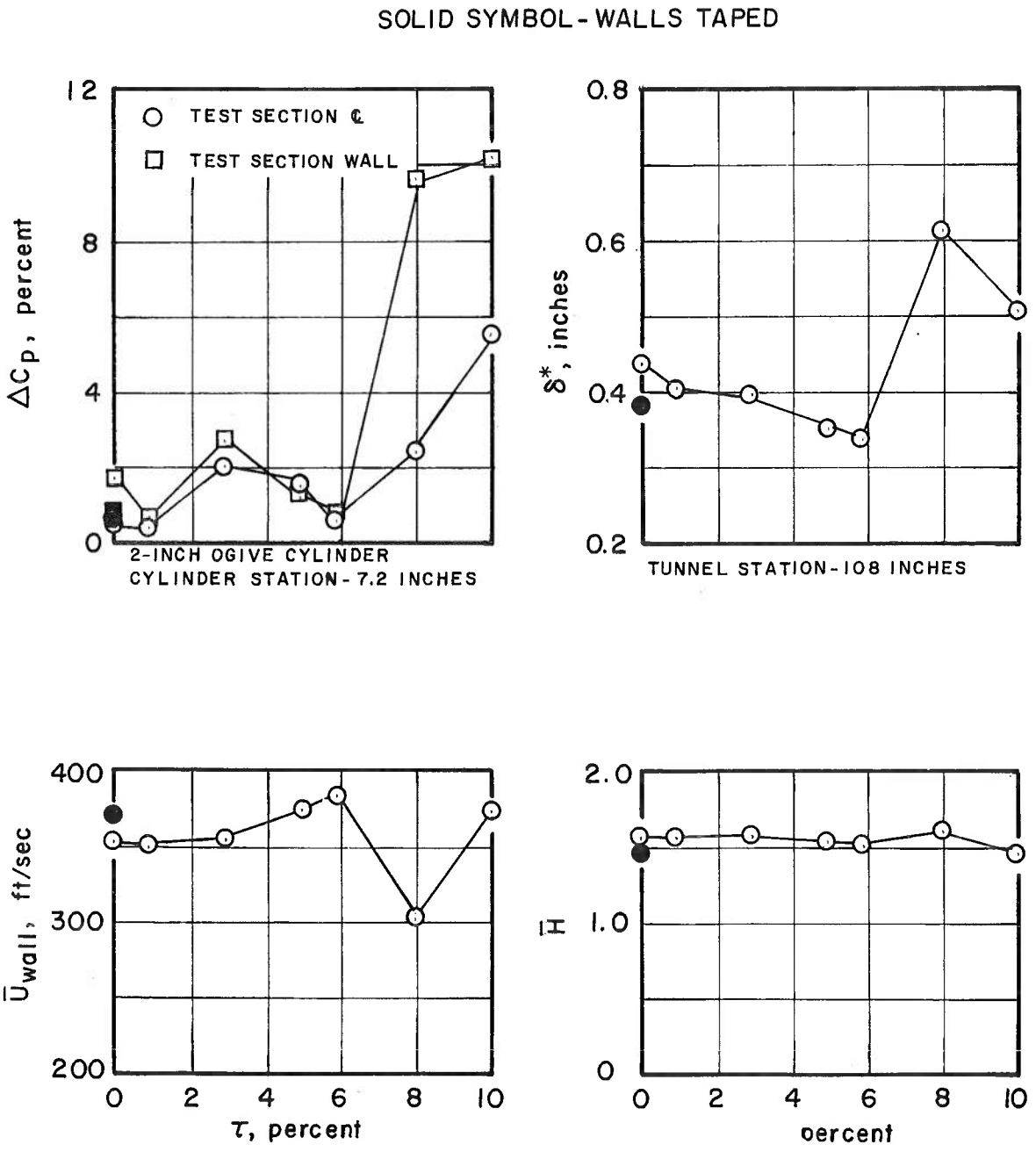

a. $M_\infty = 0.50$

Fig. 23 Variations of Tunnel 4T Wall Boundary-Layer Characteristics and Test Section Noise Levels as a Function of Wall Porosity, p_t = 1185 psfa, θ_w = 0 deg

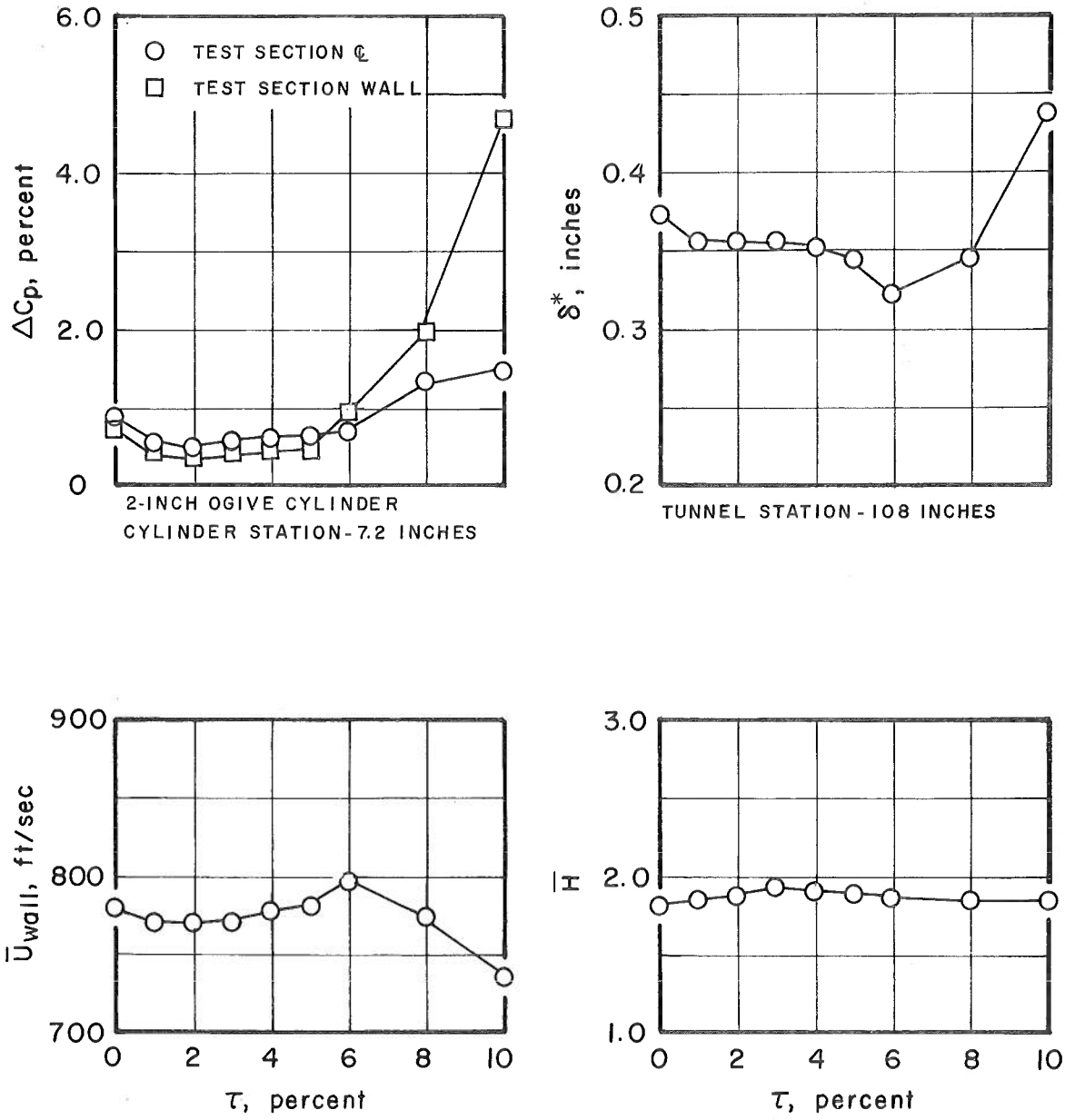

b. $M_\infty = 1.00$

Fig. 23 Continued

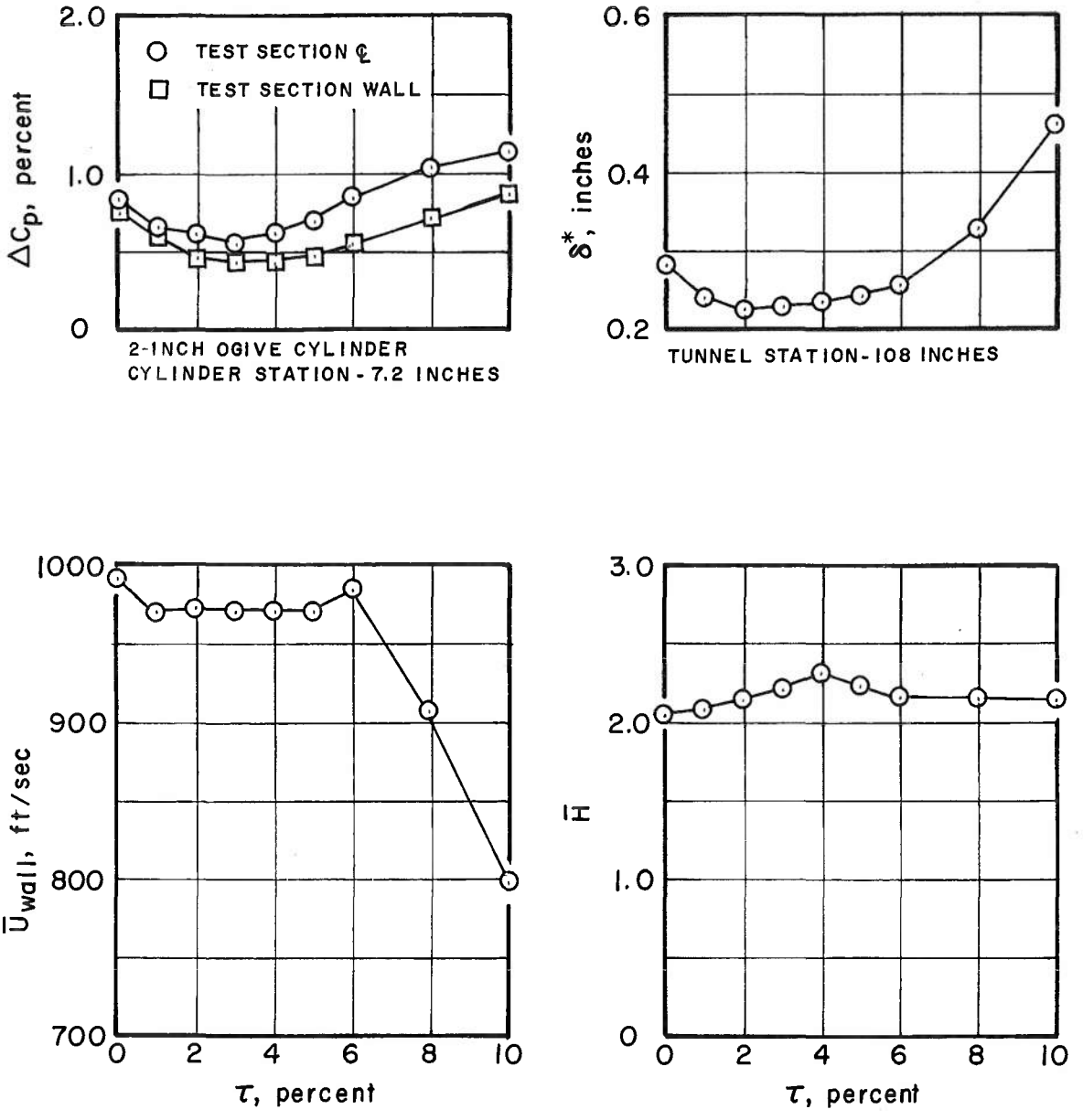

c. $M_\infty = 1.20$

Fig. 23 Concluded

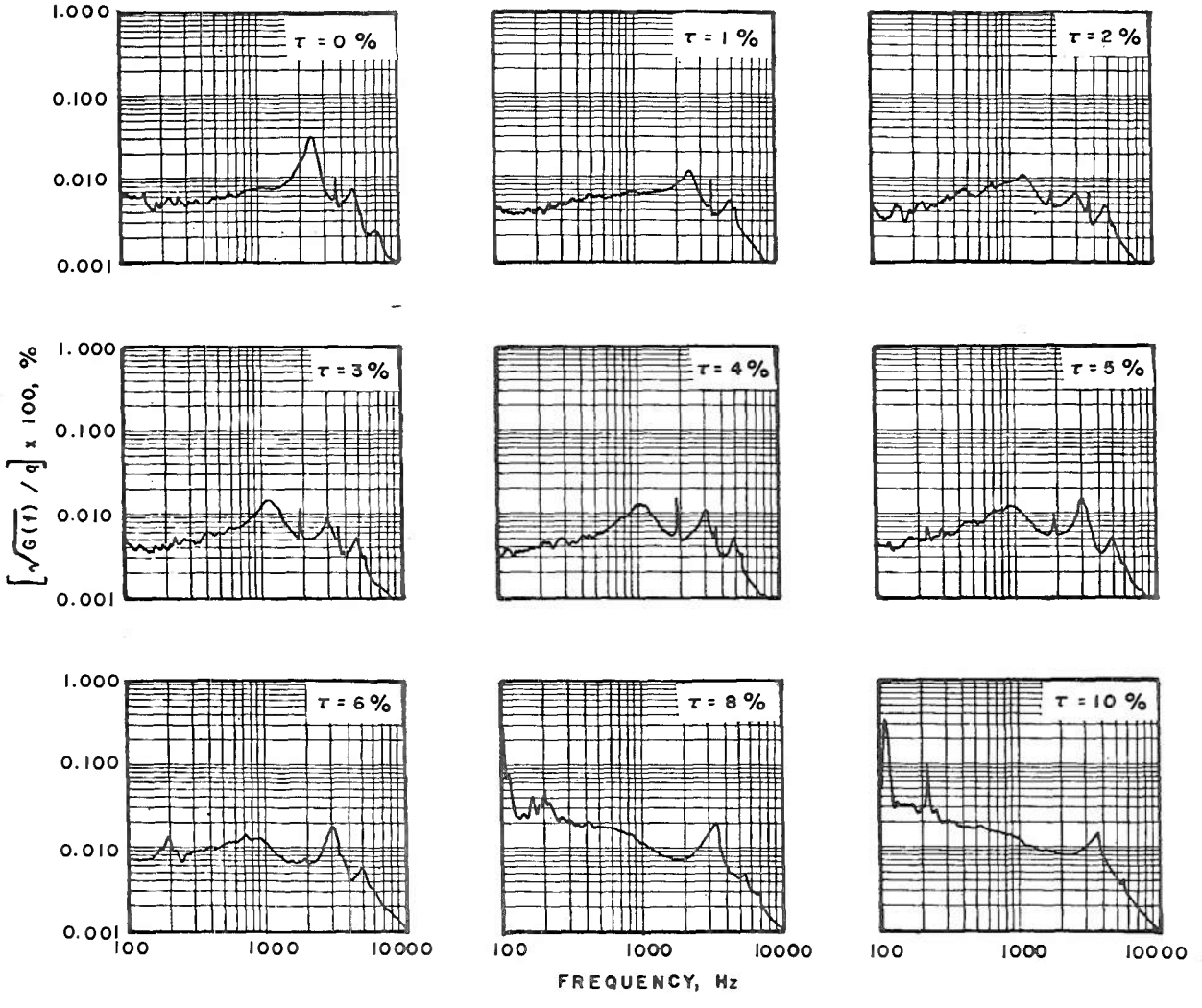

Fig. 24 Tunnel 4T Test Section Noise Spectra for Various Wall Porosities, 2-in. Ogive Cylinder, Cylinder Station 7.2 in., p_t = 1185 psfa, M_∞ = 1.00

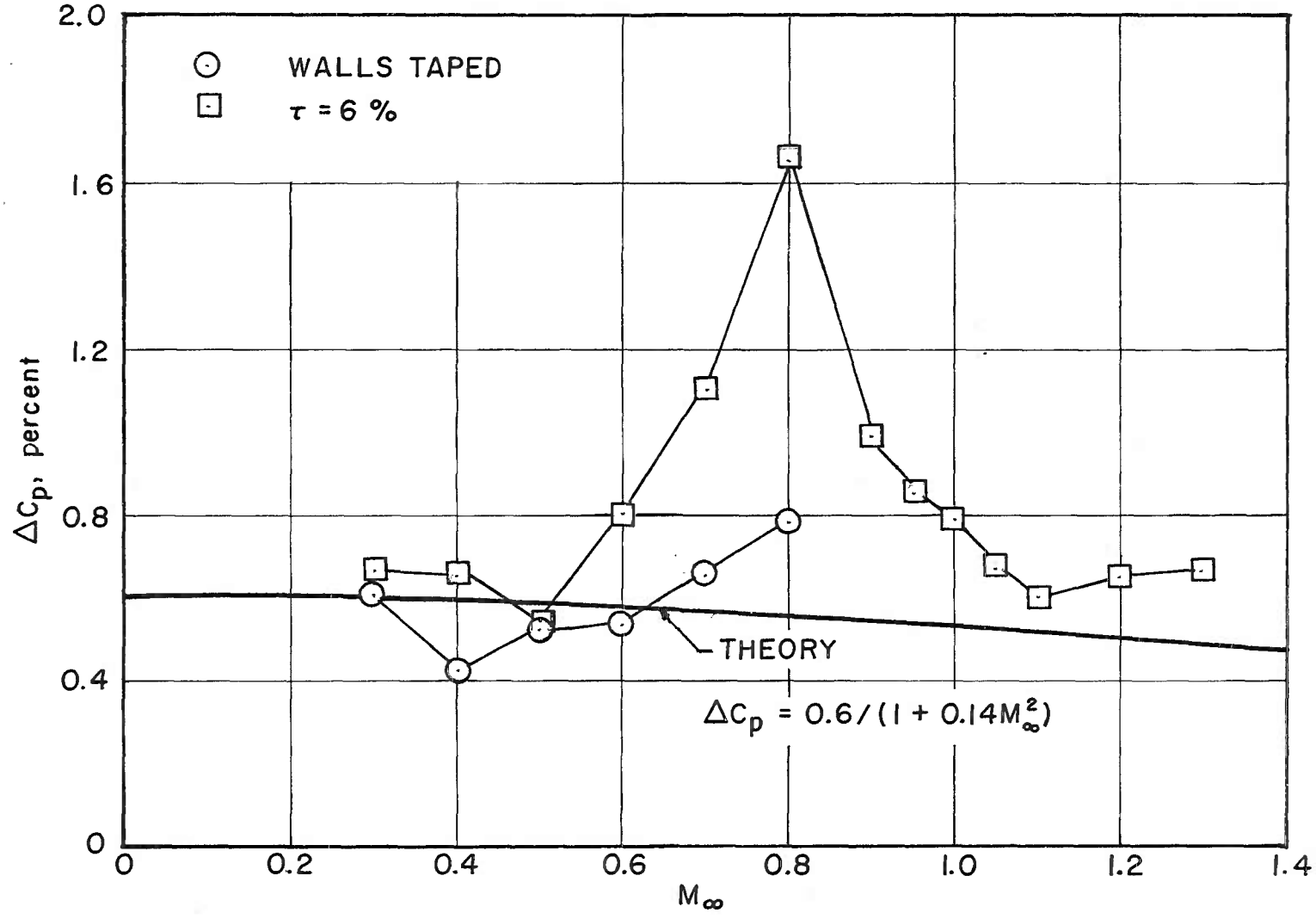

Fig. 25 Comparison of Tunnel 4T Test Section Noise Levels with Theory as a Function of M_∞, p_t = 1185 psfa

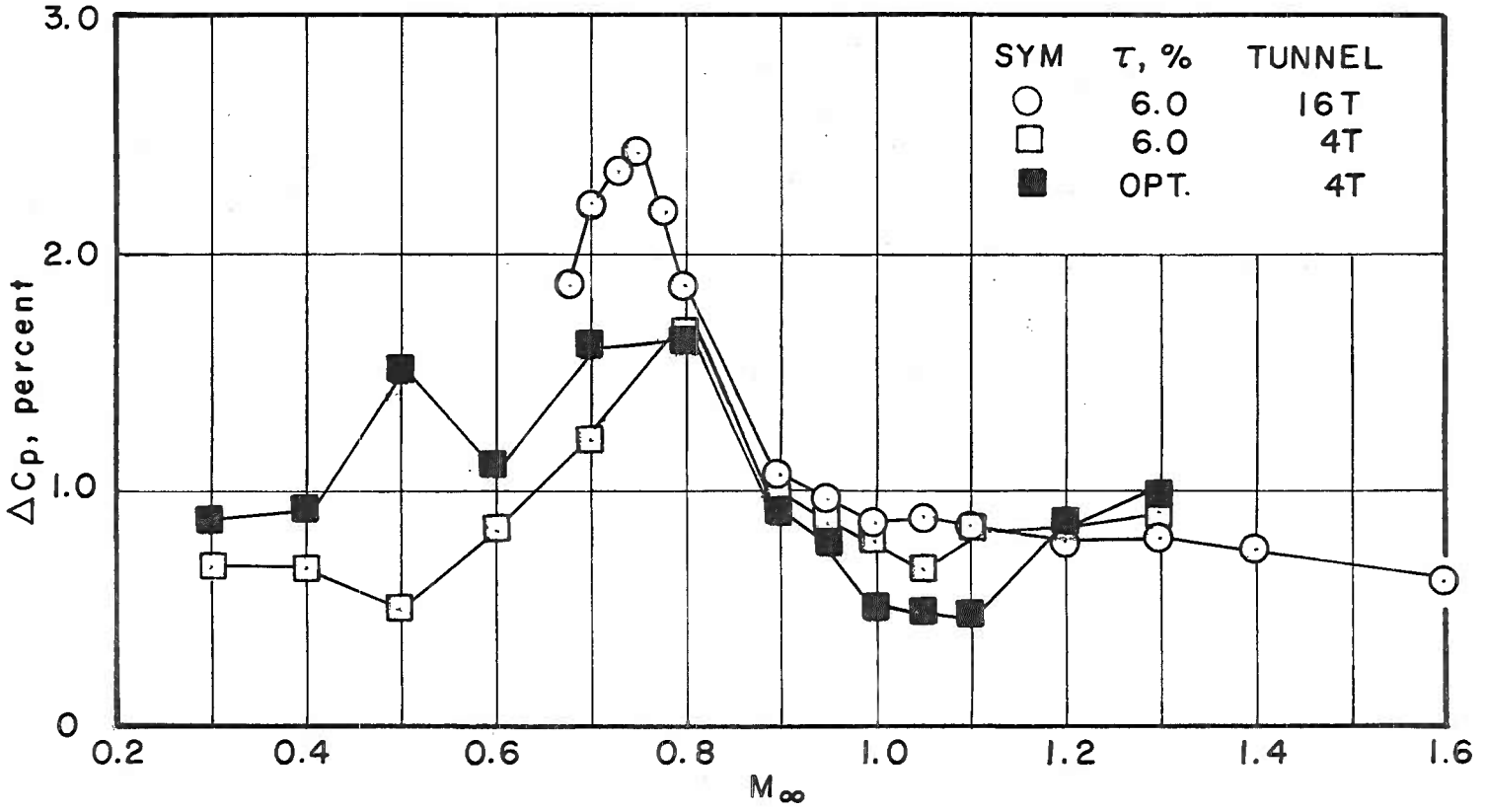

Fig. 26 Comparison of Test Section Noise Levels in Tunnels 16T and 4T, 2-in. Ogive Cylinder, Cylinder Station 7.2 in., p_t = 1185 psfa

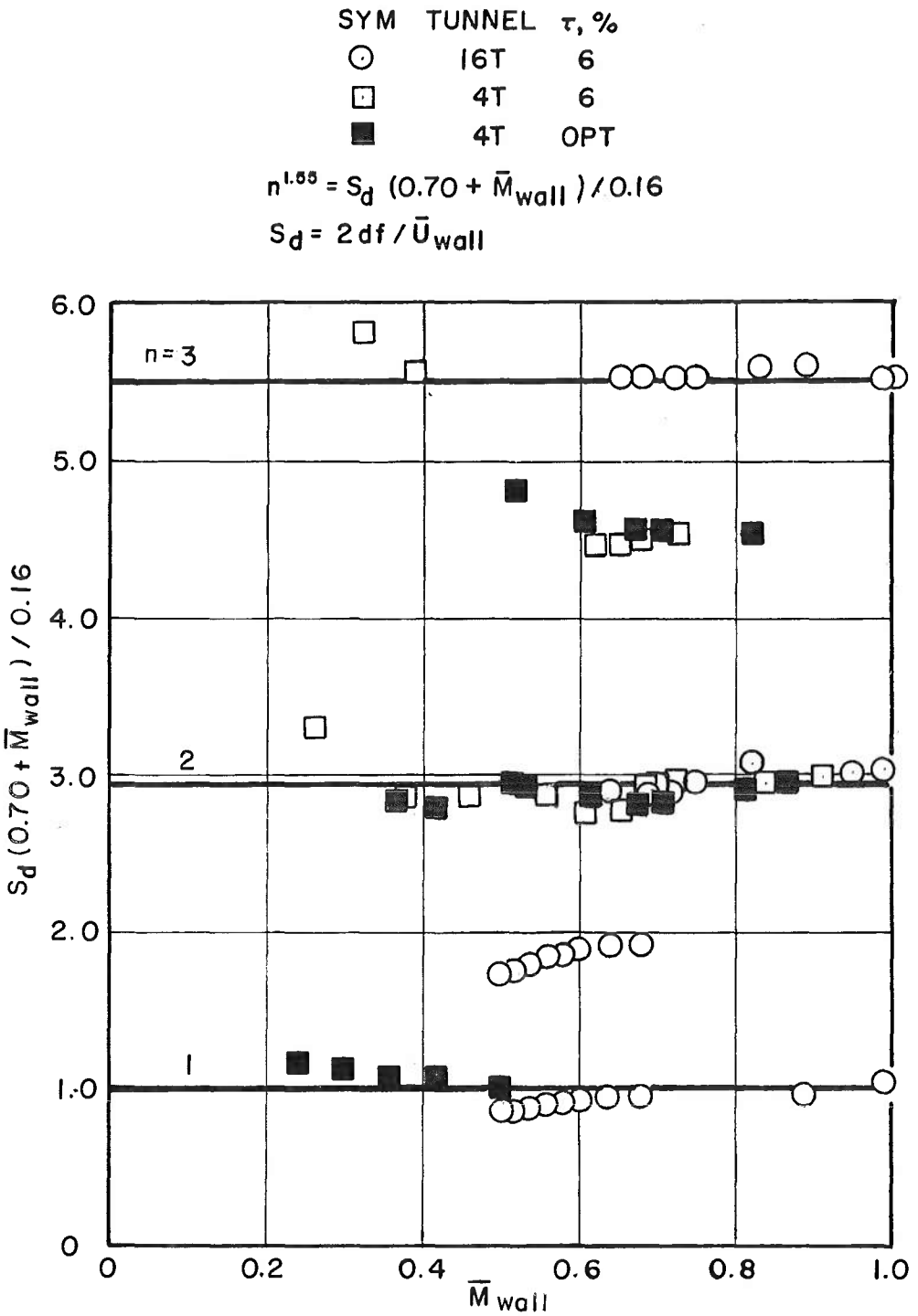

Fig. 27 Evaluation of Perforated Wall Edge Tone Frequencies in Tunnels 16T and 4T as M_∞ is Varied

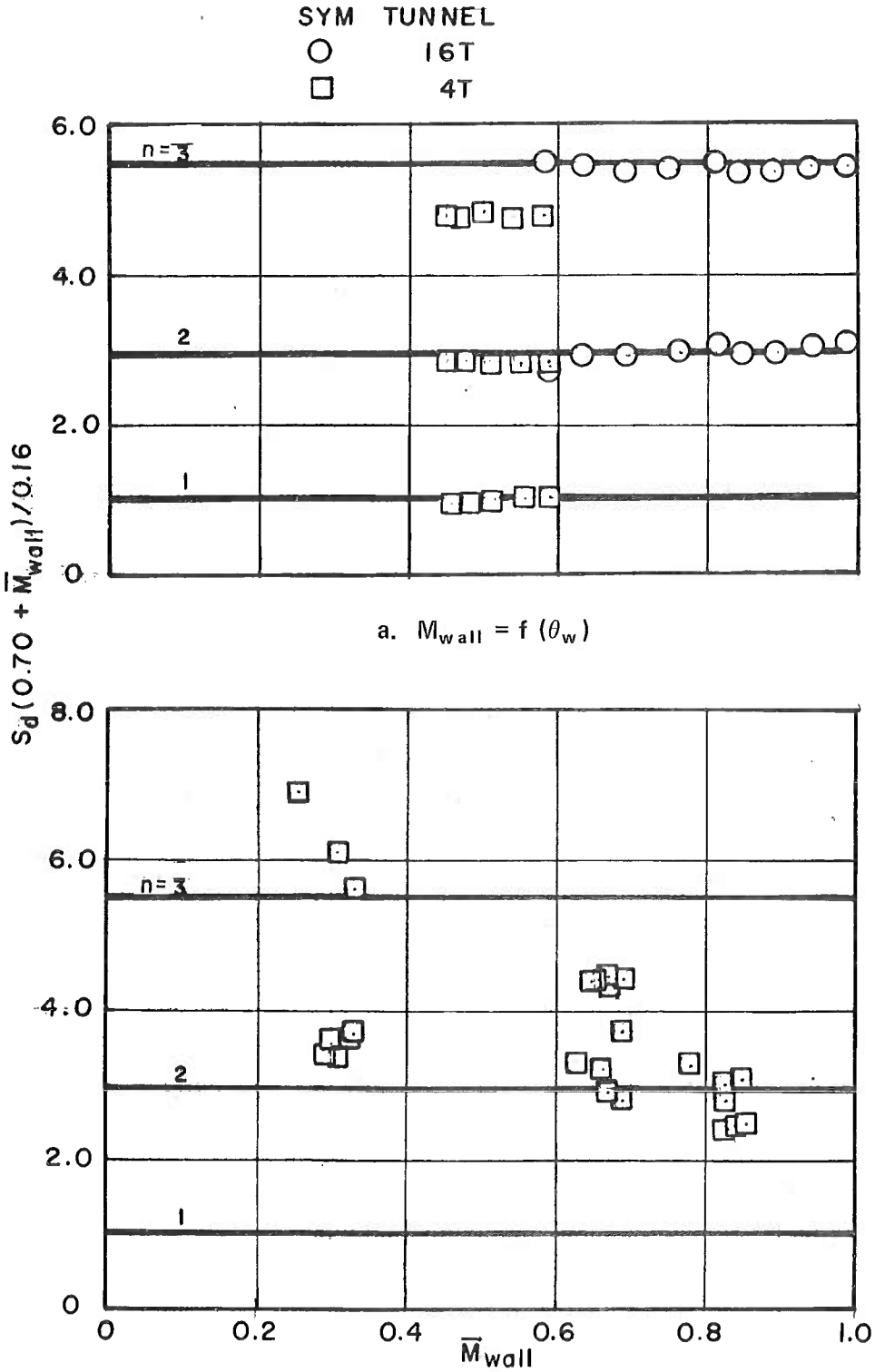

a. $M_{wall} = f(\theta_w)$

b. $M_{wall} = f(\tau)$

Fig. 28 Evaluation of Perforated Wall Edge Tone Frequencies in Tunnels 16T and 4T as θ_w and τ are Varied

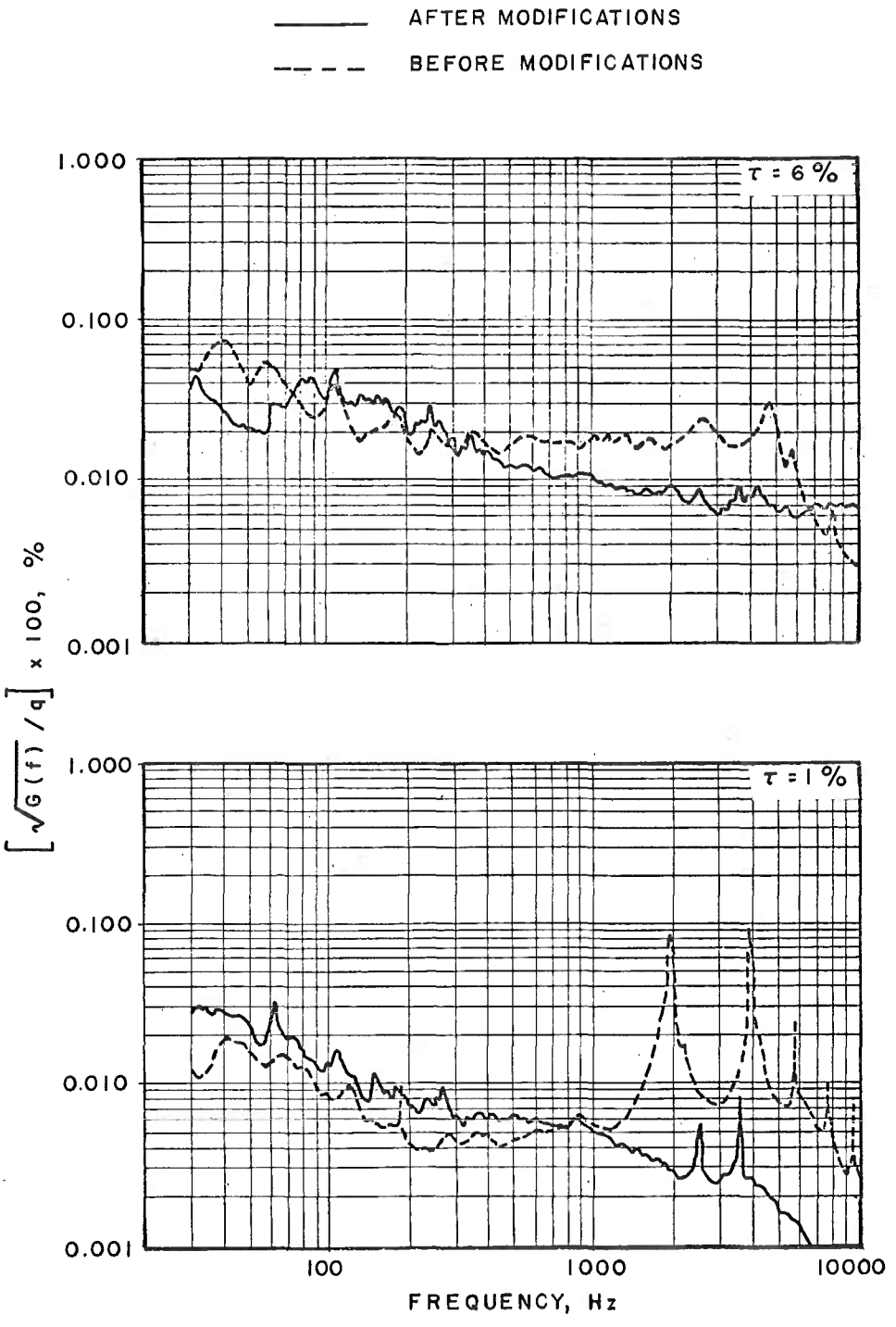

a. $M_\infty = 0.50$

Fig. 29 Evaluation of Tunnel 4T Test Section Noise Reduction attributable to Changes in Perforated Walls and Acoustically Treating the Interior of the Plenum Cavity

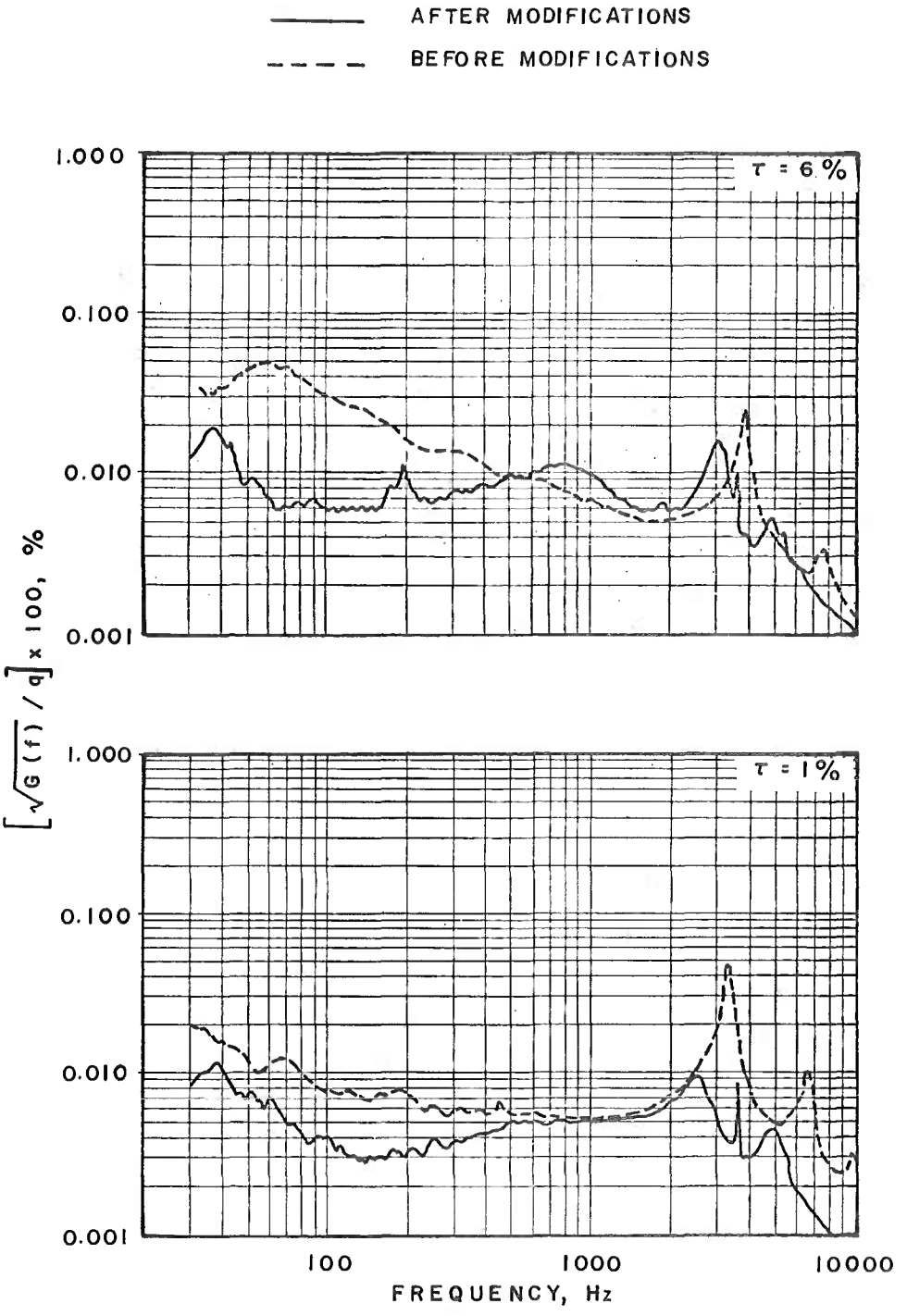

b. $M_\infty = 1.05$

Fig. 29 Concluded

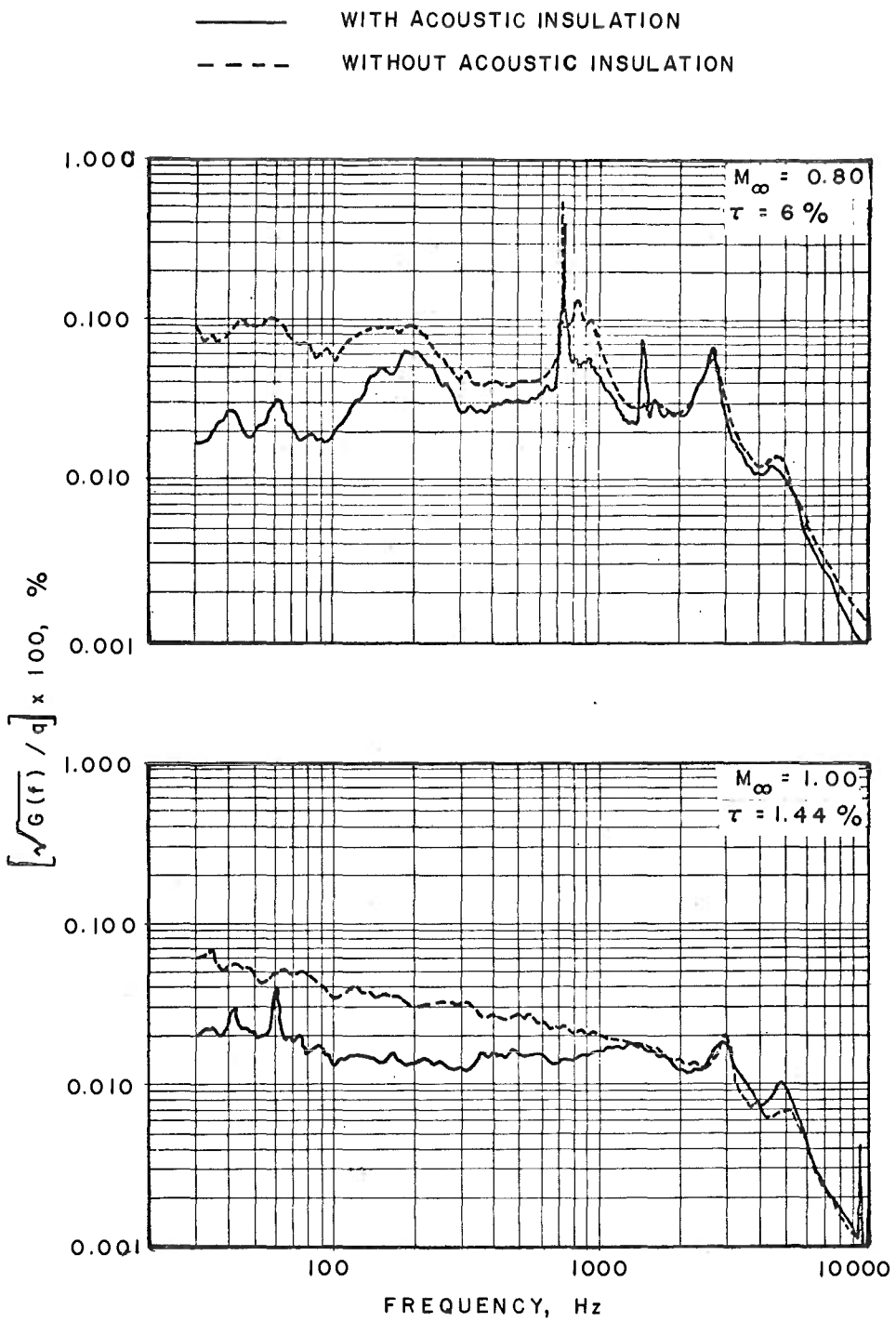

Fig. 30 Evaluation of Tunnel 4T Test Section Wall Noise before and after Acoustically Treating the Plenum Cavity

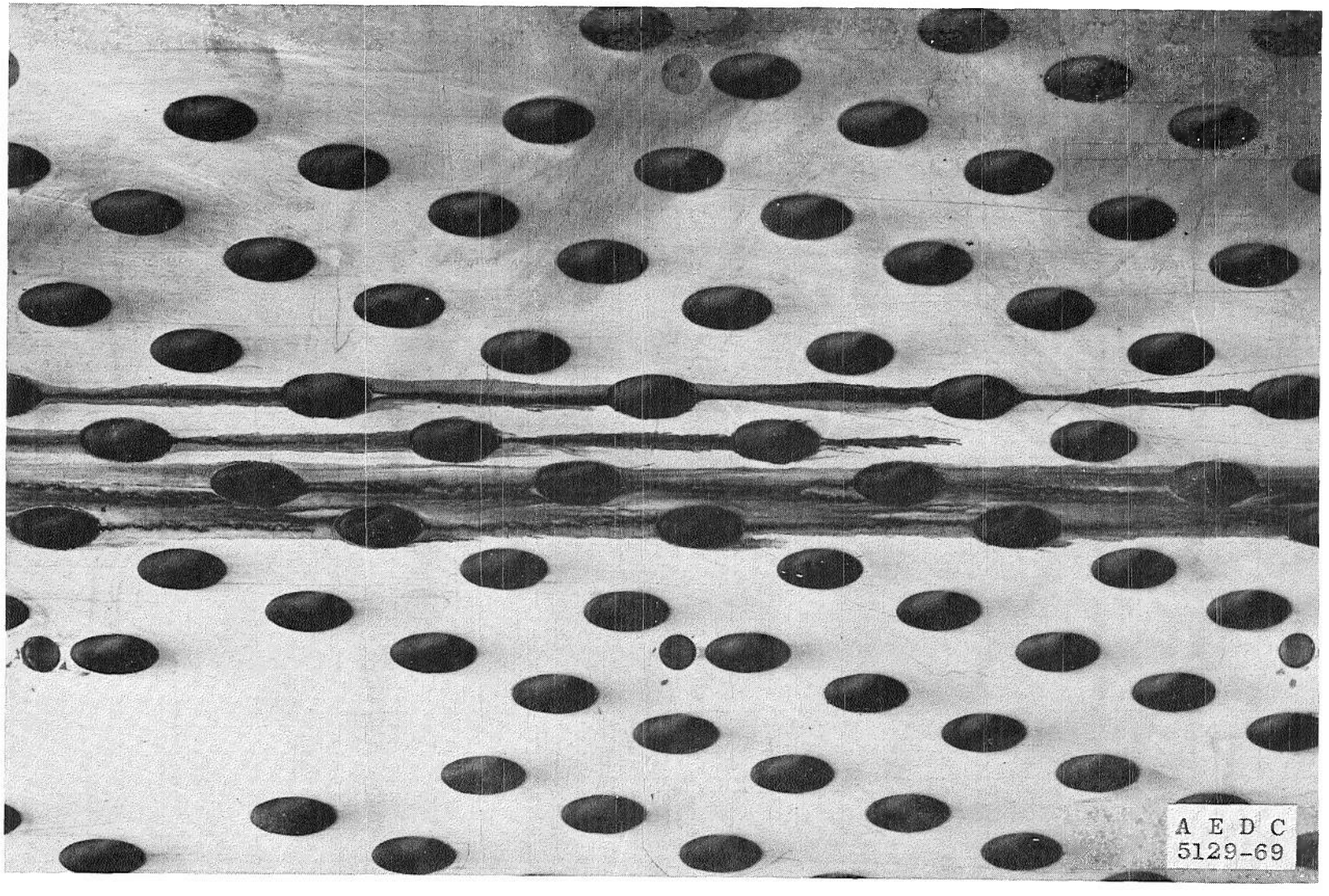

Fig. 31 Photograph of Tunnel 4T Test Section Perforated Wall with Oil Smear Flow Visualization of a Hole Vortex Formation

TABLE I
TUNNEL 4T OPTIMUM WALL
POROSITY SCHEDULE FOR NONLIFTING MODELS

M_∞	Porosity, percent
0.300 to 0.900	5.0
0.950	1.50
1.000	1.50
1.025	1.50
1.050	2.00
1.100	2.50
1.200	4.80
1.300	6.20

UNCLASSIFIED

Security Classification

DOCUMENT CONTROL DATA - R & D

(Security classification of title, body of abstract and indexing annotation must be entered when the overall report is classified)

1. ORIGINATING ACTIVITY *(Corporate author)*
Arnold Engineering Development Center
Arnold Air Force Station, Tennessee 37389

2a. REPORT SECURITY CLASSIFICATION
UNCLASSIFIED

2b. GROUP
N/A

3. REPORT TITLE
PERFORATED WALL NOISE IN THE AEDC-PWT 16-FT AND 4-FT TRANSONIC TUNNELS

4. DESCRIPTIVE NOTES *(Type of report and inclusive dates)*
Final Report, September 1969 to December 1970

5. AUTHOR(S) *(First name, middle initial, last name)*
O. P. Credle, ARO, Inc.

6. REPORT DATE	7a. TOTAL NO. OF PAGES	7b. NO. OF REFS
October 1971	71	16

8a. CONTRACT OR GRANT NO.	9a. ORIGINATOR'S REPORT NUMBER(S)
b. PROJECT NO.	AEDC-TR-71-216
c. Program Element 65401F	9b. OTHER REPORT NO(S) *(Any other numbers that may be assigned this report)*
d. System 921E	ARO-PWT-TR-71-161

10. DISTRIBUTION STATEMENT Distribution limited to U.S. Government agencies only; this report contains information on test and evaluation of military hardware; October 1971; other requests for this document must be referred to Arnold Engineering Development Center (XON), Arnold AFS, TN 37389.

11. SUPPLEMENTARY NOTES	12. SPONSORING MILITARY ACTIVITY
Available in DDC.	Arnold Engineering Development Center (XON), Arnold AFS, TN 37389

13. ABSTRACT

This report presents the results of recent studies of noise in Propulsion Wind Tunnel (16T) and Aerodynamic Wind Tunnel (4T). Noise levels in the free stream and at the test section wall were measured in both tunnels as a function of Mach number, Reynolds number, wall angle, and wall porosity. In Tunnel 4T, free-stream noise characteristics were also evaluated with solid (taped) test section walls. Test results revealed that the perforated test section wall holes generate discrete frequency, high energy noise. In Tunnel 16T, there is a critical Mach number range in which a wall hole frequency is in acoustic resonance with a compressor blade frequency. Test section noise levels were found to vary slightly with wall angle and significantly with Mach number and wall porosity. The wall porosity corresponding to the minimum noise levels was found in Tunnel 4T.

Distribution limited to U.S. Government agencies only; this report contains information on test and evaluation of military hardware; October 1971; other requests for this document must be referred to Arnold Engineering Development Center (XON), Arnold AFS, TN 37389.

DD FORM 1 NOV 65 1473

UNCLASSIFIED

Security Classification

14. KEY WORDS	LINK A ROLE	LINK A WT	LINK B ROLE	LINK B WT	LINK C ROLE	LINK C WT
2 transonic wind tunnels -- Noise						
design						
noise						
acoustic measurements						

1. Perforated walls -- Noise
wall wind tunnels --
noise

"

3

AFSC
Arnold AFS Tenn